https://doi.org/10.5194/egusphere-2026-1708
Preprint. Discussion started: 10 August 2026

Measurement report: Sources of carbonaceous aerosol in a South-East European metropolis

Stephen M. Platt[1], Milos Davidović[2], Alena Bartonova[1], Željko Ćirović[2], Sabine Eckhardt[1], Nikolaos Evangeliou[1], Hans Gundersen[1], Maja Jovanović[2], Milena Jovašević-Stojanović[2], Griša Močnik[3], Bojana Petrović[2], Philipp Schneider[1], Karl Espen Yttri[1]

[1]NILU, 2027, Kjeller, Norway
[2]VIDIS Center, Vinča Institute of Nuclear Sciences, National Institute of the Republic of Serbia, University of Belgrade, Belgrade, Serbia
[3]Center for Atmospheric Research, University of Nova Gorica, 5270 Ajdovščina, Slovenia

Correspondence to: Stephen M. Platt (sp@nilu.no)

Abstract. Carbonaceous aerosol measurements are scarce in the Western Balkans. We present year-round observations (2023 to 2025) from the urban-background site Ada Marina, Belgrade (44.790166° N, 20.4169° E; 71 m a.s.l.), combining three source apportionment (SA) approaches (organic tracers, the aethalometer model, and a novel application of non-negative matrix factorization, NNMF, to aethalometer data) with FLEXPART modelling and gridded emissions to identify source regions and transport pathways.

The annual mean equivalent black carbon (eBC) concentration was 1.42 ± 1.40 μg m^{-3}, indicating a moderate eBC burden, while PM_{10} (27.7 μg m^{-3}) remained below current EU and Serbian limits but above WHO guidelines and upcoming EU limits. All SA methods consistently show strong winter to summer seasonality driven by residential wood combustion (RWC). The aethalometer model attributes 64% of eBC to solid fuel (eBC_{SF}) in winter versus 18% in summer, NNMF yields 51% versus 6%, and offline analysis of tracers show elemental carbon from biomass burning (EC_{BB}) contributions of 48% versus 3%. Organic carbon (OC) shows similar seasonality, with biomass burning contributing 59% in winter and 4% in summer. A substantial wintertime secondary OC component linked to RWC is evident, with secondary OC (SOC) strongly correlated with EC_{BB} and eBC_{SF} (R^2 = 0.78 to 0.86), alongside enhanced brown carbon absorption (29% annually; 44% in winter). FLEXPART indicates pollution episodes are dominated by regional transport within Serbia and the Pannonian Basin, while correlations between modelled residential emissions and observations demonstrate strong model skill.

1 Introduction

Carbonaceous aerosol, predominantly black carbon (BC) and organic carbon (OC), with inorganic carbon (IC) such as carbonate carbon occasionally present, is ubiquitous and impacts health and climate. Knowledge of its ambient levels, spatiotemporal variability, physico-chemical properties, and emission sources is essential for effective air-quality management and mitigation. Following a systematic review, the World Health Organization (WHO) recommended that countries implement

https://doi.org/10.5194/egusphere-2026-1708
Preprint. Discussion started: 10 August 2026

systematic measurements of BC, including robust emission inventories and exposure assessments, and develop targeted source apportionment (SA) studies, as well as measures (including standards or targets) to reduce ambient BC concentrations (WHO, 2021). Furthermore, the revised European Union (EU) Ambient Air Quality Directive (AAQD), adopted on 23 October 2024, requires BC monitoring at both urban and rural supersites and recommends levoglucosan measurements at those sites, signalling a regulatory shift toward SA (European Parliament and Council, 2024). Even though many European locations already comply with EU limit values they still exceed the corresponding WHO guidelines. This discrepancy highlights the importance of identifying the sources that most strongly contribute to particulate pollution. In this context, the present study investigates the dominant sources of carbonaceous aerosol in Belgrade, representing one of the few year-round SA studies available for the Western Balkans.

BC is essentially soot, mainly carbon, while OC is found in organic matter (OM), comprising carbon bound with hydrogen, oxygen, and other elements (Szopa et al., 2021). IC comprises various forms of carbonate (e.g., $CaCO_3$), primarily originating from geological sources and thus commonly associated with mineral dust. BC originates from direct (primary) emissions from combustion sources such as road vehicles and residential heating or wildfires, while OC can be both primary, e.g., from combustion, or biogenic sources such as pollen and fungal spores, and secondary (formed in the atmosphere by oxidation of gaseous precursors, both anthropogenic and biogenic). BC is operationally defined as elemental carbon (EC) when measured by thermal-optical analysis, and as equivalent black carbon (eBC) when determined from optical absorption measurements (Watson et al., 2005; Petzold et al., 2013), such as from aethalometers (Drinovec et al., 2015). Another subset of carbonaceous aerosol is brown carbon (BrC), a portion of carbonaceous aerosol (often from biomass burning) that absorbs light at shorter (UV) wavelengths (Kumar et al., 2018; Marsavin et al., 2023). BrC is a mixture of complex organic compounds such as tar and humic-like substances (HULIS, Andreae and Gelencsér, 2006) and may contain BC.

Carbonaceous aerosols often represent a major fraction of PM. A recent worldwide assessment of OC and EC in PM with aerodynamic diameter of <10 µm and <2.5 µm (PM_{10} and $PM_{2.5}$, respectively) shows that their contributions vary strongly by region and particle size (Putaud et al., 2025). For example, in European PM_{10}, EC typically accounts for only about 1% of the mass, while OC contributes around 11%. In Eastern Europe this has historically been higher, Yttri et al. (2007) report carbonaceous fractions in PM_{10} of 30% at Košetice (Czech Republic) and 36% at Stará Lesná (Slovakia), both rural background sites, though more recent studies in the region are scarce. In contrast, carbonaceous material is much more abundant in $PM_{2.5}$: EC contributes consistently 7 to 9% of mass across most regions, while OC varies widely from ~10% in China and Thailand to 35 to 40% in Europe and North America. Meanwhile Putaud et al. (2025) also report that OC/PM ratios remain relatively stable, suggesting that secondary OC (SOC) is formed both in winter and summer. This highlights the strong regional dependence of carbonaceous aerosol contributions, driven by both source characteristics and atmospheric processing (e.g., SOC formation).

Carbonaceous aerosol from residential wood combustion (Skiba et al., 2024) and traffic (Platt et al., 2017) has been linked to severe health effects and ~72000 and ~35000 deaths annually in Europe, respectively (Paisi et al., 2024). Increases in BC from traffic have been linked with a higher risk of hospitalisation for coronary heart disease and a higher risk of all-cause

https://doi.org/10.5194/egusphere-2026-1708
Preprint. Discussion started: 10 August 2026

mortality (Gan et al., 2011). Furthermore, although aerosols in general have net cooling effects on climate, either directly via scattering of incoming solar radiation or indirectly via their influence on cloud formation (IPCC, 2021), BC, due to its strong light absorbing properties, also exerts a warming effect. BC warms the climate via radiative heating (Jacobson, 2002) and changes to surface albedo resulting from deposition on snow or ice (Hadley and Kirchstetter, 2012). Uncertainties in the climate effects of BC are large, mainly due to the difficulty in accurately modeling the atmospheric processing of BC and uncertainties in emissions sources (Lee et al., 2016), though also due its operational definition (Vignati et al., 2010).

Numerous source apportionment (SA) methods have been developed to disentangle contributions from biomass burning, traffic, industrial, and other sources. Traditional receptor models are widely applied to offline analyses of filter datasets, where concentrations of EC, OC, specific organic tracers, ions, metals, etc. are determined in the laboratory. Two common receptor model approaches are Chemical Mass Balance (CMB, e.g., El Haddad et al., 2011) and Positive Matrix Factorization (PMF, e.g., Chen et al., 2022; Paatero and Tapper, 1994). CMB requires source emission profiles or ratios and fits the observed aerosol composition as a linear combination of those profiles. While its strength lies in directly quantifying known sources, errors arise due to uncertainty and variability in the source profiles. Meanwhile, PMF is a data-driven approach that solves for a set of source factors and their contributions, constrained by the requirement that all contributions be non-negative (Paatero and Tapper, 1994). On the other hand, PMF results can be sensitive to methodological choices and have limitations: there is some rotational ambiguity (multiple mathematically valid solutions, Reff et al., 2007), and the model's ability to separate sources depends on having source-specific tracer species. PMF also requires sound knowledge of measurement uncertainties, which in practice are often only estimated based on instrument precision and assumptions on measurement variability, e.g., using 20% of the observed signal, as in Yttri et al. (2021), to avoid biasing results.

Non-negative matrix factorisation (NNMF), derived from the iterative update algorithm by Lee and Seung (1999) offers a flexible and computationally efficient alternative for source apportionment. It operates without requiring prior assumptions about measurement errors or uncertainty matrices, a strength when uncertainty estimates are unreliable or unavailable, though this can also be a weakness, as noisy data or outliers may disproportionately influence results. NNMF has been successfully applied to diverse atmospheric datasets: for example, it resolved indoor and outdoor particle sources in a multi-household low-cost sensor study (Rathbone et al., 2025). It has also been applied to atmospheric particle number size distributions to separate nucleation, traffic, and background aerosol modes (Liang et al., 2021). These applications demonstrate NNMF's ability to extract meaningful source factors across varying data types and conditions, with short computation times and minimal preprocessing.

In addition to composition-based techniques, SA of eBC can also be achieved by exploiting the wavelength dependence of the light absorption coefficient from which eBC is derived in the infra-red region, specifically, the absorption Ångström exponent (AAE) which describes a power law dependence of absorption on wavelength:

$$B_{ABS}(\lambda) = B_{ABS,0} \times \left(\frac{\lambda}{\lambda_0}\right)^{-AAE}, \quad (1)$$

https://doi.org/10.5194/egusphere-2026-1708
Preprint. Discussion started: 10 August 2026

where λ_0 is the reference wavelength, and $B_{ABSs,0}$ the reference absorption coefficient.

BC from lean (oxygen-rich), complete combustion of liquid fuels typically exhibits an AAE near 1 (Kirchstetter et al., 2004). In ambient air, values <1 may occur due to scattering by aged or sulfur-laden aerosols (Helin et al., 2021). AAE > 1 generally indicates the presence of light-absorbing organic species formed under fuel-rich conditions, characteristic of solid fuel burning, such as residential wood combustion or wildfires (Saleh et al., 2014). These AAE-based assumptions underpin the aethalometer model, which estimates eBC from liquid and solid fuel sources (eBC_{LF} and eBC_{SF}) using measured absorption at two wavelengths and a priori AAE values (Zotter et al., 2017; Sandradewi et al., 2008b). A major limitation of this model is its high sensitivity to the chosen AAE values. Savadkoohi et al. (2025) proposed using the 1st and 99th percentiles of observed ambient AAE distributions to represent near-pure emissions from liquid and solid sources, respectively. They reported AAE_{LF} values from 0.79 to 1.08 and AAE_{SF} from 1.45 to 1.84 across sites, noting substantial variation due to site-specific sources and background conditions. In contrast, Helin et al. (2021) reported much broader variability when directly measuring AAE at individual combustion sources, finding values from -0.2 ± 0.7 to 3.0 ± 0.8 for sources including ship engines and diesel buses. An alternative approach to optimising AAEs in the aethalometer model employs external tracers. For example, Zotter et al. (2017) used radiocarbon (^{14}C) analysis to differentiate modern (solid fuel biomass burning) from fossil carbon in Switzerland, thereby calibrating AAE values. They found relatively narrow ranges, with AAE_{LF} = 0.8 to 1.0 and AAE_{SF} = 1.6 to 1.8. AAE higher than ~2 is also observed in ambient conditions, and is linked to the presence of BrC e.g., during wildfire events (Marsavin et al., 2023). This variability highlights the degree to which AAE values are source, site, and instrument specific and cannot be generalised. Furthermore, while radiocarbon analysis provides a useful reference, it is not widely accessible due to high cost and limited access to laboratories performing radiocarbon analysis of aerosol samples. Lastly, even with optimised AAEs, the aethalometer model can yield unphysical results, such as negative source contributions. This is a predictable consequence of (i) the model's mathematical sensitivity to the exponent parameter and (ii) the temporal variability in combustion sources and atmospheric conditions, which together produce source-specific distributions of AAE values that are not adequately represented by the fixed pair of source-specific AAE values assumed in the model.

Globally, no air quality standard has yet been established for BC, nor is its monitoring mandatory. This likely contributes to the limited number of urban observational sites, despite monitoring efforts by some environmental agencies and research institutions. The resulting knowledge gap regarding carbonaceous aerosols and SA is particularly pronounced in South-East Europe and the Western Balkans (e.g., Serbia, Bosnia and Herzegovina, and North Macedonia), where accessible data for regional- and local-scale SA remain scarce.

In many countries of this region, biomass burning for residential heating is widespread due to the affordability and availability of wood (Sopčić et al., 2025). The adoption of vehicle emission regulations also lags behind the rest of Europe, with most vehicles meeting Euro 4 standards or lower (World Bank, 2024). This is partly attributable to the import of second-hand vehicles, which account for more than 80% of passenger car imports (Munoz-Raskin et al., 2025), while the rollout of electric vehicles and associated infrastructure has been slow (Pajic et al., 2024). In this context, it is important to assess the impact of

https://doi.org/10.5194/egusphere-2026-1708
Preprint. Discussion started: 10 August 2026

the recent regulatory amendment in Serbia requiring imported vehicles to meet the Euro 6 standard from 1 January 2025 (Republic of Serbia, 2023).

Emissions from traffic and residential wood combustion are further exacerbated by stagnant wintertime meteorological conditions, and studies consistently identify biomass burning and traffic as dominant PM sources in Balkan cities (Sopčić et al., 2025). In Belgrade, source apportionment analysis of offline chemically speciated PM indicates a strong influence of wood smoke during colder months, alongside traffic contributions throughout the year (Petrović et al., in Prep.). The health impacts of carbonaceous PM in this region are therefore severe, accounting for at least 129 000 disability-adjusted life-years (WHO, 2019). Several Western Balkan countries rank among the highest in Europe for mortality attributable to air pollution (Belis et al., 2019). Despite these issues, there has historically been a lack of extensive, long-term monitoring of carbonaceous aerosol in the Western Balkans suitable for source apportionment. Many air quality networks in the region, e.g., that of the Serbian Environmental Protection Agency (SEPA) focus on PM mass, basic gaseous pollutants (SO_2, NO_2), as well as BC, without including multiwavelength measurements or chemical speciation (SEPA, 2025).

Recent studies nevertheless highlight the importance of carbonaceous particulate matter in Serbia. Measurement campaigns in central Belgrade have reported high concentrations of organic carbon (OC) and elemental carbon (EC) in winter, for example on-line measurements (aethalometer and total carbon analyzer, TCA) during winter campaign in city center of Belgrade before COVID-19 pandemic reported mean OC concentrations of 7.78 µg C m^{-3} and eBC of 4.43 µg m^{-3} within $PM_{2.5}$ with organic matter as a large $PM_{2.5}$ component (~27%), underscoring the central role of carbonaceous aerosol in ambient fine particles (Jovanović et al., 2020). Earlier source apportionment work in Belgrade also identifies strong biomass-burning influences on urban OA during a campaign performed from October to December 2008 (Zangrando et al., 2016a; Zangrando et al., 2016b). Within this regional context, we focus on Belgrade, the largest city in the Western Balkans, and present an online year-round dataset (June 2023 to February 2025, of online eBC measurements, via aethalometer, AE33) and offline chemical analyses (EC, OC, and organic tracers) available for Serbia. Motivated by the known limitations of the aethalometer model, we explore a data-driven approach to eBC source apportionment using NNMF. We apply both the traditional aethalometer model and NNMF to the eBC dataset and evaluate their performance using tracer-based source apportionment of the offline filters. From the filter analysis, we resolve elemental carbon (EC) and organic carbon (OC) into biomass burning (EC_{BB}, OC_{BB}) and fossil fuel (EC_{FF}, OC_{FF}), and primary biological aerosol particles (OC_{PBAP}) and secondary organic carbon (OC_{SOC}) contributions. This integrated approach, combining high-time-resolution optical data with detailed chemical speciation, provides a robust framework for source apportionment, essential for understanding urban air pollution and supporting effective mitigation strategies in the region.

2 Methodology

In this study we combine offline analysis and source apportionment of carbonaceous aerosol components collected on filters between 06 June 2023 and 29 May 2024, online aethalometer (AE33) measurements spanning 23 October 2023 to 11 February

https://doi.org/10.5194/egusphere-2026-1708
Preprint. Discussion started: 10 August 2026

2025, and air mass transport modelling combined with gridded emissions for the full period (Fig. 1). Although OC/EC filter sampling extends beyond this interval (see Sect. 2.2.4) the time series is restricted here to the period for which additional tracers (e.g., levoglucosan) were available, enabling integrated source apportionment.

We use the overlapping period between offline and online data (23 October 2023 to 29 May 2024) for intercomparison of SA approaches. Both the offline and online datasets span approximately one year, providing a sufficient basis for comparison with annual means as typically used in regulatory frameworks (e.g., Serbian and EU limit values, WHO air quality guidelines). I.e., while their exact periods differ, both are suitable for assessment against such annual metrics.

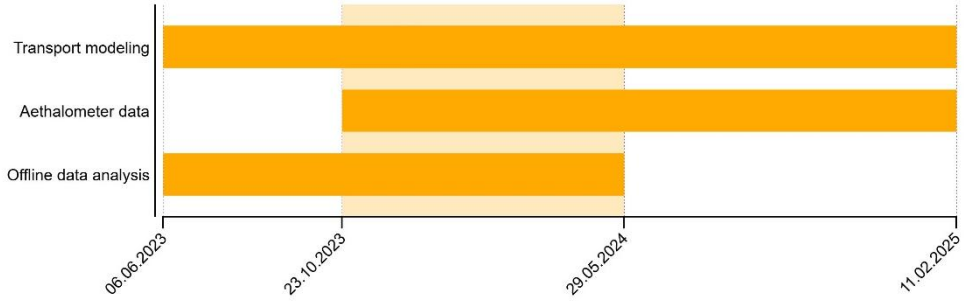

Figure 1: Data availability. Offline filter analyses (OC/EC and tracers) span 06 June 2023 to 29 May 2024 (dates shown in format DD.MM.YYYY); online aethalometer eBC spans 23 October 2023 to 11 February 2025; transport modelling (FLEXPART footprints) covers the full study period. The shaded band marks the overlap period between offline and online (23 October 2023 to 29 May 2024).

For clarity, we adopt the following terminology throughout this study:

- Offline dataset: filter-based OC/EC and tracer analyses spanning 06 June 2023 to 29 May 2024.
- Online dataset: aethalometer eBC measurements spanning 23 October 2023 to 11 February 2025.
- Overlap period: the concurrent period of 23 October 2023 to 29 May 2024, used for intercomparison of source apportionment approaches.

Seasonal references:

- For the offline dataset, seasonal coverage is limited to summer 2023, autumn 2023, winter 2023 and 2024, and spring 2024.
- For the online dataset, seasonal coverage extends further, including summer 2024, autumn 2024, and winter 2024 and 2025 in addition to the periods above.

2.1 Site description

Measurements were conducted at Ada Marina (44.790166° N, 20.4169° E; 71 m a.s.l.), an urban background site located at Ada Ciganlija in the Banovo Brdo neighbourhood of southwestern Belgrade (population ~1.4 million; greater metropolitan

https://doi.org/10.5194/egusphere-2026-1708
Preprint. Discussion started: 10 August 2026

area ~1.7 million), near the confluence of the Sava and Danube rivers (Fig. 2). The site is part of the Serbian Environmental Protection Agency (SEPA) automatic air quality monitoring network (SEPA, 2025).

The station lies approximately 300 to 500 m south of the E-75 motorway and the Most na Adi bridge, both major traffic corridors and important local emission sources. Additional nearby sources include residential wood combustion (RWC), particularly during the heating season, and industrial activity in the New Belgrade district, which lies upwind under prevailing westerly winds. A natural gas–fired residential heating plant is located ~1.5 km to the west, and Belgrade Nikola Tesla Airport (~10 km northwest), one of the busiest airports in the Balkan Peninsula, may contribute episodically.

To the east, the Vinča municipal landfill and dense urban traffic (approximately 0.7 million registered passenger cars and 90 000 trucks) represent additional emission sources. Further southwest, the Nikola Tesla coal-fired power plant complex is located ~25 km away, with associated lignite mining basins and an additional power plant near the Lazarevac municipality of Belgrade. Broader regional influences include the Smederevo steel plant (~30 km east) and the Kostolac coal-fired power plant

https://doi.org/10.5194/egusphere-2026-1708
Preprint. Discussion started: 10 August 2026

(~50 km northeast). Surrounding agricultural areas may also contribute to episodic aerosol loading through soil resuspension and agricultural waste burning.

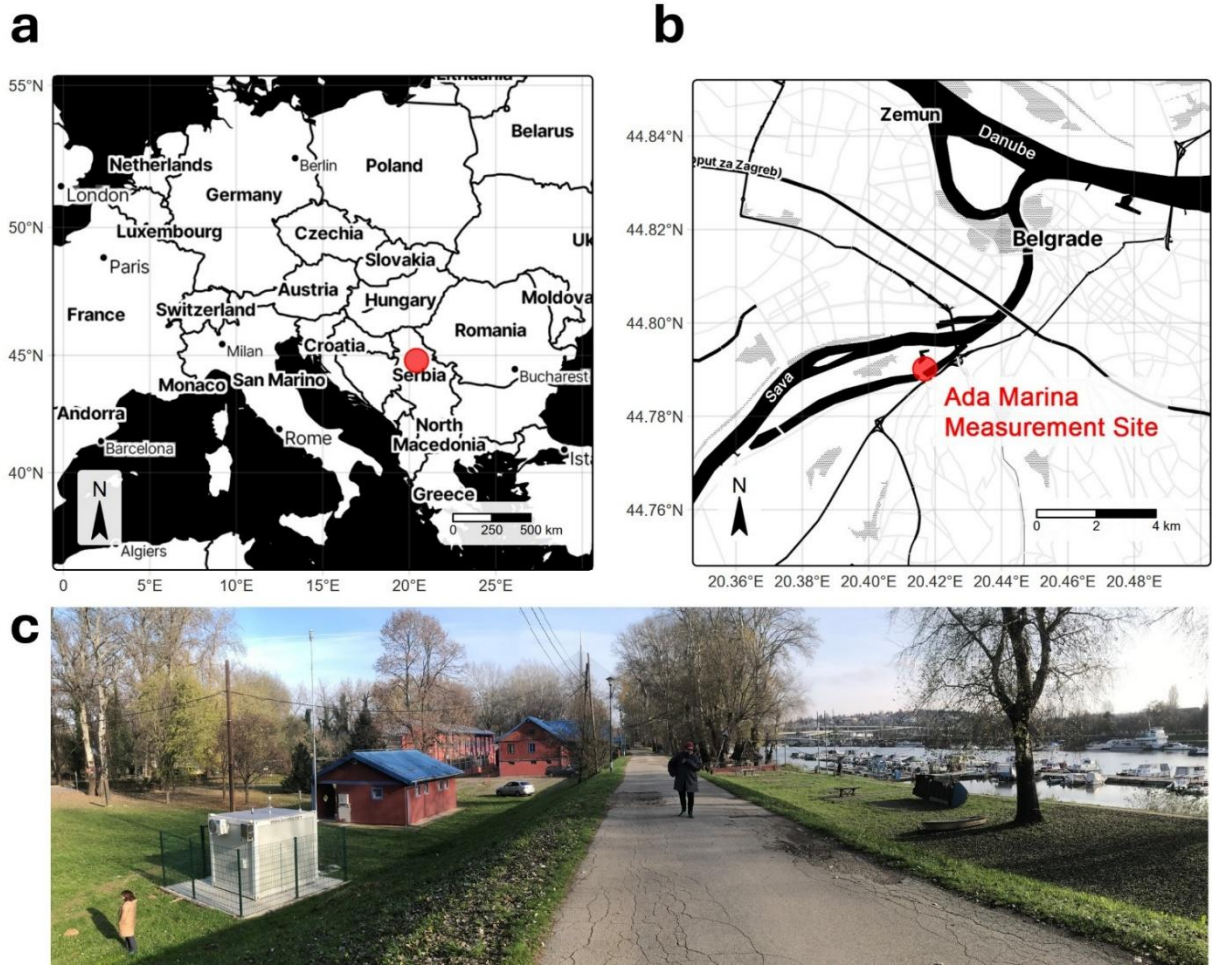

Figure 2: Study location in Belgrade. (a) Regional map of Europe with Belgrade highlighted. (b) City-scale map marking the Ada Marina urban-background measurement site (red dot) on the Sava lakeshore (Ada Ciganlija). (c) Site photograph: the measurement site is the white building on the left; Sava Lake is on the right (photo: Stephen M. Platt). Base maps © OpenStreetMap contributors; tiles © Stamen Design (CC BY 3.0).

2.2 Measurements

2.2.1 Absorption and equivalent black carbon (eBC)

We performed multiwavelength (λ=370, 470, 520, 590, 660, 880, 950 nm) measurements with a filter absorption photometer (AE33 aethalometer, Magee), which measures light attenuation across a filter tape (attenuation coefficient, $B_{ATN,}$) to determine the aerosol absorption coefficient (B_{ABS}). We used tape type M8060, hence we divide attenuation B_{ATN} by a harmonisation factor (H*) of 1.76 following ACTRIS recommendations (ACTRIS, 2021). The aethalometer sampled from a $PM_{2.5}$ inlet with

https://doi.org/10.5194/egusphere-2026-1708
Preprint. Discussion started: 10 August 2026

excess flow. We determined eBC at 880 nm from B_{ABS} at 880 nm using a mass absorption cross section (MAC) of 7.57±0.51 m² g⁻¹, the slope of orthogonal distance regression to the EC time series,

$$eBC_{\lambda=880\ nm} = \frac{B_{Abs,\lambda=880\ nm}}{MAC_{\lambda=880\ nm}} \quad . \qquad (2)$$

We found good agreement between B_{ABS} at 880 nm and EC, with (pseudo) R^2=0.87 (computed from vertical residuals), while the intercept was not statistically different from zero at -0.38±0.52 Mm^{-1}. Our derived MAC value is consistent with the instrument default value of 7.77 m² g⁻¹ (Drinovec et al., 2015) and the average reported by Savadkoohi et al. (2025) from 12 European sites, 7.8±3.4 m² g⁻¹, validating its use in this study.

As described by Drinovec et al. (2015), the AE33 aethalometer employs an automatic two-spot loading compensation algorithm to correct for the filter loading effect, which results in a non-linearity-reduction of sensitivity with the amount of sample on the filter. When properly applied, this algorithm ensures that eBC concentrations remain independent of the baseline B_{ATN}. Consequently, for a sufficiently large dataset, a plot of B_{ABS} versus B_{ATN} should exhibit a near-zero slope. However, for very long time series, e.g. 1 year, the terminating B_{ATN} at 880 nm varies with the seasonal pattern in AAE since terminating attenuation is set by B_{ATN} at 370 nm, with lower terminating B_{ATN} at 880 nm in winter when AAE is generally higher (Fig. S1). At the same time, concentrations are generally higher in winter, leading to a bias in of B_{ABS} versus $B_{ATN,}$ whereby higher concentrations appear associated with lower B_{ATN} at 880 nm. To explore this wavelength-dependent and seasonally varying tape-advance behaviour, we analyse B_{ABS} at 880 nm as a function of fractional spot completion, defined using the attenuation at 880 nm as B_{ATN} / $B_{ATN,\,MAX}$. When B_{ABS} at 880 nm is binned by fractional spot completion, no systematic dependence of B_{ABS} at 880 nm on B_{ATN} / $B_{ATN,\,MAX}$ is observed (Fig. S2), indicating that the dual-spot loading correction using the BC(B_{ATN}) dependence performs as intended. Hence, we did not apply any posterior corrections to the two-spot algorithm. Note also that B_{ATN} / $B_{ATN,MAX}$ cannot be used for such correction.

2.2.2 Aerosol filter samples

Three ambient aerosol filter samples were collected every second day from 31 May 2023 to 30 May 2024 using three co-located, identical low-volume samplers (LVS3, Leckel) equipped with PM_{10} inlets. Filter samples, from 'Sampler 1' were used for chemical analysis, whereas those from 'Sampler 2' were used for gravimetric analysis. Sampler 3 was a backup sampler not used in the current study. Quartz fibre filters (PALLFLEX Tissuequartz 2500QAT-UP, 47 mm diameter) were pre-conditioned for 48 h at 20±1 °C and 50±1 % relative humidity prior to sampling to allow subsequent gravimetric determination of PM_{10} mass.

Before sampling, filters were stored in polystyrene Petri dishes at 4 °C. Three field blanks per month were obtained by placing filters in the sampler housing without initiating airflow, to account for contamination during handling and transport. Following gravimetric analysis, these filters were stored at −20 °C pending further chemical analysis. Filters from Sampler 1 were stored at −20 °C immediately after sampling and were used for OC, EC, and organic tracer analyses.

2.2.3 Thermal-optical analysis of elemental and organic carbon

https://doi.org/10.5194/egusphere-2026-1708
Preprint. Discussion started: 10 August 2026

Organic carbon (OC) and elemental carbon (EC) were measured from filters collected by Sampler 1 by thermal-optical analysis using a Sunset Laboratory OC/EC aerosol analyzer. The instrument operated according to the EUSAAR-2 temperature protocol (Cavalli et al., 2010), using optical transmission correction for charring.

2.2.4 Organic tracers

Organic tracers (Table 1) were analysed using ultra-high-performance liquid chromatography (UHPLC; Vanquish UHPLC, Thermo Fisher Scientific) coupled with a Q Exactive™ Plus Orbitrap mass spectrometer (Thermo Fisher Scientific), following the method described by Yttri et al. (2024).

A subset of samples from Sampler 1 was selected using a distribution-preserving approach designed to ensure representativeness of the full chemical variability. For this purpose, a composite weighted time series was constructed to give equal weight to ionic, metallic, and carbonaceous components:

$$x_{\text{weighted}} = \frac{x_{\text{ions}}/\sum x_{\text{ions}} + x_{\text{metals}}/\sum x_{\text{metals}} + x_{\text{C}}/\sum x_{\text{C}}}{3} \quad (3)$$

For each month, seven samples were selected corresponding to the minimum, maximum, and the 10th, 25th, 50th (median), 75th, and 90th percentiles of this metric. This ensured that the full monthly statistical distribution of bulk chemical composition was represented in the tracer analysis. In total, 84 exposed filter samples and 6 field blanks were analysed for tracers. Note: the combined time series of OC/EC and tracers begin on 06 June 2023 and ends 29 May 2024, resulting in the offline analysis period shown in Fig.1. The analysis of metals and inorganic ions is described elsewhere (Petrović et al., in preparation) and is not presented in detail here.

Table 1: Organic tracers analysed in this study and their source categories.

Organic tracers	Sources
Levoglucosan, mannosan galactosan	Biomass Burning (BB)
Arabitol, mannitol, fructose, glucose, trehalose	Primary Biological Aerosol Particles (PBAP)
2-methylerythritol, 2-methylthreitol	Biogenic Secondary Organic Aerosol from oxidation of isoprene ($BSOA_{Isoprene}$)

2.3 Source apportionment

2.3.1 Aethalometer model

To improve the applicability of the aethalometer model (Sandradewi et al., 2008) under real-world conditions, we adopted an optimised approach using ambient observed absorption Ångström exponents (AAE) AAE percentiles, as proposed by Tobler et al. (2021) and formalised by Savadkoohi et al. (2025). In this method, the AAE for liquid fuel (AAE_{LF}) and solid fuel (AAE_{SF}) combustion are not fixed a priori but are instead inferred from the statistical distribution of observed bulk AAE values. Specifically, it is assumed that:

https://doi.org/10.5194/egusphere-2026-1708
Preprint. Discussion started: 10 August 2026

- The 1st percentile (P1) of the AAE distribution (AAE_{P1}) corresponds to periods dominated by liquid fuel combustion, yielding AAE_{LF}.
- The 99th percentile (P99, AAE_{P99}) reflects near-pure solid fuel combustion, yielding AAE_{SF}.

A strict criterion requiring a coefficient of determination $R^2>0.99$ was applied to the log–log linear fit of absorption vs. wavelength for AAE values to be considered valid in the percentile analysis. This ensures that only high-confidence spectral fits influence the percentile-derived AAE values.

Savadkoohi et al. (2025) note that during winter months the bulk data may be unlikely to contain any AAEs representative of a pure liquid fuel source. Therefore, we obtain P1 based solely on the distribution seen in summer (June, July, August). These percentile-derived AAE values are then applied in the aethalometer model (Eqs. 4 and 5, Zotter et al., 2017; Sandradewi et al., 2008b) using the wavelength pair λ=520 nm and λ=880 nm:

$$B_{ABS_{LF}}(\lambda = 880\ nm) = \frac{B_{ABS}(\lambda=520\ nm) - B_{ABS}(\lambda=880\ nm) \times \left(\frac{520}{880}\right)^{-AAE_{P1}}}{\left(\frac{520}{880}\right)^{-AAE_{P99}} - \left(\frac{520}{880}\right)^{-AAE_{P1}}}, \quad (4)$$

$$B_{ABS_{SF}}(\lambda = 880\ nm) = \frac{B_{ABS}(\lambda=520\ nm) - B_{ABS}(\lambda=520\ nm) \times \left(\frac{520}{880}\right)^{-AAE_{P99}}}{\left(\frac{520}{880}\right)^{-AAE_{P1}} - \left(\frac{520}{880}\right)^{-AAE_{P99}}}, \quad (5)$$

The same MAC value is assumed for both liquid and solid fuel time series (Zotter et al., 2017; Sandradewi et al., 2008b).

2.3.2 Non-negative matrix factorisation

We implemented a custom NNMF routine to apportion spectral absorption data into source-related components (see Platt, 2026, and code availability). The input is a two-dimensional matrix V, representing absorption coefficients at multiple wavelengths (columns) over time (hourly, rows). This approach assumes that a bulk data matrix V of i rows and j columns (here $V = B_{ABS}$, i=t=time, j=λ=wavelength) is approximated by the sum of non-negative factors of number or rank R:

$$B_{ABS_{t,\lambda}} \approx (WH)_{t,\lambda} = \sum_{a=1}^{R} W_{t,a}\, H_{a,\lambda}\,, \quad (6)$$

Here, R=2, i.e., liquid fuel and solid fuel (Fig. S4), though an R=3 solution was explored (Fig. S5).

2.3.3 Initialisation

To generate a seed profile for H, a random AAE between 0.6 and 3 was drawn for each factor, and the initial spectral profiles in H were generated accordingly by constructing power-law curves (normalised to unity at 370 nm). This approach produces realistic starting spectra while maintaining variability across ensemble runs, improving stability compared to purely random positive seeding. The temporal profiles in W were initialized randomly from a uniform distribution and constrained to be positive.

2.3.4 Iterative algorithm

NNMF iterations (n) were performed using the classical multiplicative update rules by Lee and Seung (1999), proceeding as follows:

https://doi.org/10.5194/egusphere-2026-1708
Preprint. Discussion started: 10 August 2026

$$H^{n+1} \leftarrow H^n \odot \left(\frac{(W^n)^T V}{(W^n)^T W^n H^n} \right), \quad (7)$$

$$W^{n+1} \leftarrow W^n \odot \left(\frac{V (H^{n+1})^T}{W^n H^{n+1} (H^{n+1})^T} \right), \quad (8)$$

where $\odot$ denotes element-wise multiplication, T demotes the transposed matrix, and the divisions are also elementwise. Conceptually, this algorithm iteratively rescales the temporal (W) and spectral (H) matrices such that their product WH converges toward the observed absorption matrix V, while preserving non-negativity. Each iteration adjusts the factor profiles and their temporal contributions in proportion to the mismatch between reconstruction and observation, thereby progressively minimising the reconstruction error, $B_{ABS_{t,\lambda}} - (WH)_{t,\lambda}$. Negative values arising from numerical error were replaced with a small floor value (1×10^{-10}) to maintain strict non-negativity.

2.3.5 Performance metrics

Unlike the aethalometer model, NNMF does not prescribe fixed AAE values but allows them to emerge from the data, while retaining the physically meaningful non-negativity constraint. At each iteration, AAEs were therefore calculated by fitting a linear regression in log–log space to each row of H (log absorption vs. log wavelength). The fractional contribution of each factor to absorption at 880 nm ($f_{a(\lambda=880\ nm)}$), was also tracked:

$$f_{a(\lambda=880\ nm)} = \frac{W_a H_{a,\lambda=880nm}}{\sum_{a'=1}^{R} W_{a'} H_{a',\lambda=880\mathrm{nm}}}, \quad (9)$$

2.3.6 Convergence

Convergence was assessed using residual diagnostics rather than reconstruction error alone. Normalised residuals (E) were defined as:

$$E_{(t,\lambda)} = \frac{V_{t,\lambda} - (WH)_{t,\lambda}}{V_{t,\lambda}}, \quad (10)$$

and summarised by the median residual across all times at each wavelength (Fig. S4c). To ensure comparability across wavelengths with different magnitudes, medians were normalised by the interquartile range (IQR) of the corresponding observed column in V. This metric is less sensitive to outliers and it prevents high-absorption channels (370, 470 nm) from dominating. Convergence was declared when all wavelength-specific median residuals were simultaneously (i) close to zero ($|\ \mathrm{median}\ |/\mathrm{IQR} < 0.003$) and (ii) stable between iterations (<0.002 change) for at least three consecutive iterations.

Exploratory runs showed that both AAE and factor contributions evolve rapidly during early iterations and become gradual and monotonic after ~30 iterations. Each run was therefore required to perform a minimum of 30 iterations; convergence typically occurred within ~500 iterations, although a maximum of 5000 iterations was allowed. These convergence criteria were chosen to ensure stability rather than optimisation of a specific solution and yielded comparable factor structures across independent ensemble runs (Fig. S4).

2.3.7 Ensemble approach and solution stability

https://doi.org/10.5194/egusphere-2026-1708
Preprint. Discussion started: 10 August 2026

To minimise dependence on initialisation and assess rotational ambiguity, the NNMF was repeated 500 times. Accepted runs were combined using the element-wise median of W and H, providing a robust ensemble solution resistant to outlier fits. Factors were sorted by AAE before this ensemble aggregation.

Diagnostics from the ensemble are shown in Fig. S4. The AAE distributions of the final solution from each run form two narrow and well-separated modes (Fig. S4a), indicating stable factor identification with minimal rotational ambiguity. The corresponding factor-share distributions are also distinct (Fig. S3b), demonstrating limited degeneracy between components. Residual probability distributions (Fig. S4c) are centred near zero across all wavelengths, with narrow symmetric shapes, indicating that the two-factor solution captures the dominant structure of the absorption dataset without systematic bias. Together, these diagnostics support adoption of the two-factor solution for subsequent analysis.

Although NNMF is implemented here using an iterative optimisation framework, the underlying concept is simple: the observed absorption matrix is decomposed into two non-negative spectra and their corresponding time series whose product reconstructs the measurements. The ensemble approach is used primarily to ensure robustness against initialisation rather than to introduce methodological complexity. In practice, the solution behaves similarly to a constrained two-component regression, but with the advantage that spectral shapes are inferred directly from the data.

2.3.8 Synthetic data testing

As an additional validation step, the NNMF ensemble approach was applied to a synthetic dataset comprising two source components with prescribed spectral slopes (AAE ≈ 1.00 and ≈ 1.90), including ~1% Gaussian noise and realistic seasonal variability in the solid-fuel contribution. The recovered factor AAEs (1.05 and 1.85, Fig. S6) agreed closely with the imposed values (1.00 and 1.90), with deviations of less than 0.1, indicating robust recovery of source-specific spectral signatures under mixed and noisy conditions.

2.3.9 Brown carbon

BrC was determined following the approach of e.g., Basnet et al. (2024); (Massabò et al., 2015), whereby BrC is estimated by extrapolating the light absorption apportioned eBC at longer wavelengths back to shorter wavelengths and assigning the excess to BrC. This approach assumes eBC absorption dominates at 880 nm, where organic aerosol absorption is negligible. The eBC absorption at 370 nm, $B_{ABS,eBC}(\lambda = 370)$, can then be estimated by extrapolating from λ=880 nm using a fixed absorption Ångström exponent for eBC (AAE_{eBC}):

$$B_{ABS,eBC}(\lambda = 370) = B_{ABS}(\lambda = 880) \times \left(\frac{370}{880}\right)^{-AAE_{eBC}}, \quad (11)$$

where $B_{ABS}(\lambda = 880)$ is the measured absorption at 880 nm and AAE_{eBC} was set to 1.0, a value typical for fresh, fossil fuel-related black carbon (Kirchstetter et al., 2004; Sandradewi et al., 2008b). BrC at 370 nm is then determined by subtraction:

https://doi.org/10.5194/egusphere-2026-1708
Preprint. Discussion started: 10 August 2026

$$B_{ABS,BrC}(\lambda = 370) = B_{ABS}(\lambda = 370) - B_{ABS,eBC}(\lambda = 370), \quad (12)$$

2.3.10 Tracer Analysis

We apportioned carbonaceous aerosol into biomass burning (BB) and fossil fuel (FF) contributions by means of observed concentrations of OC (OC_{TOT}), EC (EC_{TOT}), and the biomass burning tracer levoglucosan (levo). This method relies on established emission ratios between levoglucosan and EC, $\left(\frac{EC}{Levo}\right)_{BB}$, and between levoglucosan and OC, $\left(\frac{OC}{Levo}\right)_{BB}$, to estimate OC_{BB} and EC_{BB}. EC_{FF} was calculated as the residual EC after subtracting EC_{BB}, and the corresponding OC_{FF} by using a representative $\left(\frac{OC}{EC}\right)_{FF}$ emission ratio for fossil fuel combustion.

Biomass burning contributions to EC_{TOT} and OC_{TOT} (EC_{BB}, OC_{BB}) were then calculated as:

$$EC_{BB} = Levo \times \left(\frac{EC}{Levo}\right)_{BB}, \quad (13)$$

$$OC_{BB} = Levo \times \left(\frac{OC}{Levo}\right)_{BB}, \quad (14)$$

and fossil fuel contributions to EC_{TOT} and OC_{TOT} (EC_{FF} , OC_{FF}) according to:

$$EC_{FF} = EC_{TOT} - EC_{BB}, \quad (15)$$

$$OC_{FF} = EC_{FF} \times \left(\frac{OC}{EC}\right)_{FF}, \quad (16)$$

Emission ratios vary both spatially and temporally. To account for this variability, we performed a Monte Carlo (MC) simulation with 1,000,000 iterations. In each iteration, the following parameters were randomly sampled: $\left(\frac{EC}{Levo}\right)_{BB}$, $\left(\frac{OC}{Levo}\right)_{BB}$, and $\left(\frac{OC}{EC}\right)_{FF}$, using a BetaPERT distribution to generate random noise, allowing for a distribution bounded by lower, upper, and central values from the literature (Table 2).

An upper $\left(\frac{OC}{Levo}\right)_{BB}$ ratio was derived from the lowest observed OC_{TOT}/ levoglucosan ratio seen at Ada Marina of 9.7, which aligns with reported values across Europe, including: 12.6±3.1 north of the Alps and 7.8±2.7 south of the Alps in Switzerland, 7.24±0.03 in Austria, 5.62±0.3 in the Po Valley (Zotter et al., 2014, and references therein), and 11.1 and 12.7 for Norway (Yttri et al., 2021). Although the ratio of 9.7 corresponds to a period dominated by residential wood burning, contribution from other sources cannot be entirely excluded. However, the concurrent low concentrations of sugars, sugar alcohols, and 2-methyltetrols, suggests only minor influence from PBAP and biogenic SOA (BSOA). Notably, 2-methyltetrols are oxidation products of isoprene and thus indicative of BSOA, but do not necessarily reflect contributions from anthropogenic precursors. To account for this potential interference, we applied a ratio ranging from 5.6 to 9.7, using the midpoint (7.65) as the central

https://doi.org/10.5194/egusphere-2026-1708
Preprint. Discussion started: 10 August 2026

value in OC_{BB} calculations. This range is consistent with literature values and serves as a precautionary measure to maintain the robustness of subsequent calculations.

For $\left(\frac{EC}{Levo}\right)_{BB}$, we derived a minimum ratio of 1.1 from the Ada Marina dataset based on minimum EC_{TOT}/levoglucosan, which is consistent with the range reported by Zotter et al. (2014) for central and southern Europe (0.87 to 1.72). From this, we adopted 0.87 as the lower bound and 1.1 as the upper bound of the EC/levoglucosan ratio range, using the midpoint (0.985) as the central value for calculating EC_{BB}.

While the calculations for OC_{FF} and OC_{BB} are intended to represent primary emissions, distinguishing these from secondary organic aerosol remains challenging. Emissions are complex gaseous and particulate mixtures that undergo evaporation, condensation, and chemical transformation in the atmosphere, blurring the distinction between primary and secondary sources (Robinson et al., 2007). Nevertheless, this differentiation may still prove useful, e.g., in assessing their relative toxicity. We thus applied a broad range (0.2 to 1.3) with a central value of 0.6, when calculating OC_{FF}, adopting the range used by both Gilardoni et al. (2011) and Yttri et al. (2011).

As a consistency check, we also estimated OC associated with primary biological aerosol particles (OC_{PBAP}) and secondary organic carbon (SOC), allowing for a full mass closure of the carbonaceous aerosol. Using five selected sugars and sugar alcohols (Arabitol, mannitol, fructose, glucose, and trehalose), we estimated an $\left(\frac{OC}{\sum Sugars, sugar\ alcohols}\right)_{PBAP}$ ratio of 8.8 from the Ada Marina dataset after correcting for contributions from OC_{BB} and OC_{FF}. To assess the influence of OC_{SOC}, we assumed it accounted for 10 to 50% of OC_{Tot}. This adjustment yielded a lower bound $\left(\frac{OC}{\sum Sugars, sugar\ alcohols}\right)_{PBAP}$ ratio of 3.9 at 50% OC_{SOC} and 7.8 at 10% OC_{SOC}. For calculating OC_{PBAP}, we adopted a range from 3.9 to 8.8, using their average (6.4) as the central value. PBAP contributions to OC (OC_{PBAB}) were then calculated as:

$$OC_{PBAP} = \sum sugars, sugar\ alcohols \times \left(\frac{OC}{\sum Sugars, sugar\ alcohols}\right)_{PBAP}, \quad (17)$$

whereas OC_{SOC} was estimated as the residual according to:

$$OC_{SOC} = OC_{TOT} - OC_{BB} - OC_{FF} - OC_{PBAP}, \quad (18)$$

Lastly, a 25% uncertainty was assumed on all measured parameters and randomly sampled in the Monte Carlo simulation according to a gaussian distribution.

Table 2: Minimum, central, and maximum values used in the BetaPERT distribution for resampling of parameters in the Monte Carlo estimation of uncertainties in the tracer-based source apportionment.

Parameter	Description	Min	Central value	Max
$\left(\frac{OC}{Levo}\right)_{BB}$	OC from biomass burning per unit levoglucosan	5.6	7.65	9.7

https://doi.org/10.5194/egusphere-2026-1708
Preprint. Discussion started: 10 August 2026

$\left(\frac{EC}{Levo}\right)_{BB}$	EC from biomass burning per unit levoglucosan	0.87	0.985	1.1
$\left(\frac{OC}{EC}\right)_{FF}$	OC from fossil fuel per unit fossil EC	0.2	0.6	1.3
$\left(\frac{OC}{\sum Sugars, sugar\ alcohols}\right)_{PBAP}$	OC per sum of PBAP tracers (Arabitol, mannitol, fructose, glucose, trehalose)	3.9	6.4	8.8

2.4 Airmass transport modelling

We used the model FLEXPART version 10.4 (Pisso et al., 2019) within the ATMO-ACCESS Research Infrastructure (https://www.atmo-access.eu) framework to track air mass transport and investigate the possible origin of BC during the study period. FLEXPART releases computational particles at heights 0 to 100 m from the receptor (Ada Marina) that are tracked backward in time, following the ambient flow as defined by hourly reanalysis meteorological fields (ERA5) from the European Centre for Medium-Range Weather Forecasts (ECMWF) with 137 vertical levels (up to approximately 80 km) and a horizontal resolution of 0.5°×0.5° (Hersbach et al., 2020). The tracking considers gravitational settling for spherical particles, dry and wet deposition of aerosols (Grythe et al., 2017) turbulence (Cassiani et al., 2015) unresolved mesoscale motions (Stohl et al., 2005) and deep convection (Forster et al., 2007). Simulations extended 30 days backward in time, which is sufficient time to include >98% of BC and OC emissions arriving at the station, given a typical lifetime of 1 week (Bond et al., 2013).

The model output consists of a species-specific footprint emission sensitivity (FES) that expresses the probability of any emission occurring in each grid-cell to reach the receptor. The footprint can be converted to modelled concentration at the receptor, when coupled with gridded emissions from an emission inventory. Anthropogenic emissions were adopted from the UNECE Convention on Long-Range Transboundary Air Pollution (LRTAP) dataset (Klimont, 2024) at high spatial resolution (0.1°×0.1°). Wildfire emissions were adopted from the Copernicus Global Fire Assimilated System (CAMS GFAS, Kaiser et al., 2012). This product was preferred against other available public ones, because it provides an estimation of the injection altitude of the fire emissions that is crucial for accurate simulation of the plume dispersion.

The BC emissions product is available at https://atmo-access.nilu.no/AdaMarina_SRB.py, and includes BC emissions from the residential sector (cooking and heating, labelled 'DOM' in the online product), transportation excluding shipping ('TRA'), shipping ('SHP'), waste management ('WST'), agricultural and wildfire ('Fire BC'), gas flaring ('FLR'), and industrial ('IND').

https://doi.org/10.5194/egusphere-2026-1708
Preprint. Discussion started: 10 August 2026

3 Results and discussion

3.1 Elemental carbon, organic carbon, and tracer-based source apportionment

The Monte Carlo (MC) source apportionment framework was applied to the full offline filter analysis period and separated by season to resolve the temporal variability in carbonaceous aerosol sources, including fossil fuel (FF), biomass burning (BB), primary biological aerosol particles (PBAP), and secondary organic carbon (SOC, Fig. 3). The MC approach demonstrated that even when accounting for uncertainties in emission ratios and Eqs. 13 to 18 the resulting uncertainty estimates are relatively narrow (shown as probability density functions, PDF, in Fig. S3). Annual and seasonal concentrations of carbon fractions and organic tracers used as inputs, along with source apportionment results, are presented in Table 3.

EC from fossil fuel combustion (EC_{FF}) consistently dominated EC year-round (Fig. 3b), contributing 79% on average (Table 3). However, the contribution from EC_{BB} increased markedly in winter to 48%, approximately equalling EC_{FF}, consistent with increased levoglucosan emissions from RWC. OC_{SOC} (48%) dominated OC annually, followed by OC_{BB} (27%), OC_{PBAP} (16%), and OC_{FF} (9%). Primary anthropogenic sources, particularly OC_{BB}, average 59%, dominated in winter. There was notable contribution from OC_{SOC} also in winter of 33%. Given the low biogenic activity during this period, it is likely of anthropogenic origin, with RWC as the most plausible source due to its pronounced seasonal pattern. The higher correlation of OC_{SOC} with OC_{BB} ($R^2 = 0.78$) than with OC_{FF} ($R^2 = 0.34$) in winter further supports an RWC origin (of wintertime OC_{SOC}). Concentrations of 2-methyltetrols, which are oxidation products of isoprene, were 35 times lower in winter than in summer, indicating negligible influence of isoprene-derived BSOA. Oxidation products of monoterpenes, such as 3-MBTCA (3-methylbutane-1,1,3-tricarboxylic acid) and pinic acid, observed in measurements from Kanal (Slovenia), 500 km away (Glojek et al., 2024), exhibit much less seasonal variability. Thus, while a contribution from monoterpene-derived BSOA cannot be excluded, it is still unlikely to dominate wintertime OC_{SOC}. OC_{PBAP} peaked in summer, reflecting the seasonal biological cycle, and was second only to OC_{SOC} during this period. A substantial fraction (21 to 44%) of OC_{PBAP} was apportioned to fungal spores, based on emissions ratios reported by Bauer et al. (2002). The mannitol to arabitol ratio (1.1±0.3) for Ada Marina was consistent with that of fungal spores (1.5±0.5) found by Bauer et al. (2002), as well as with what has been reported for ambient aerosol collected across Europe (Yttri et al., 2024; Yttri et al., 2021; Yttri et al., 2011).

The annual mean PM_{10} concentration of 27 μg m^{-3} at Ada Marina (for overlapping samples from Sampler 1 and Sampler 2, see Sect. 2.2.4, Fig. 4) is below the current EU and Serbian annual limit value of 40 μg m^{-3} (European Parliament and Council, 2024; Republic of Serbia, 2023). National monitoring in Serbia reports annual PM_{10} concentrations exceeding the limit value at multiple (8 out of 52) stations in 2023, including Valjevo (60 μg m^{-3}), Zaječar (52 μg m^{-3}), and several urban locations (SEPA, 2024). Consequently, the Ada Marina site can be considered relatively clean compared to many urban and industrial monitoring locations across the country. However, Ada Marina appears somewhat polluted in a European context (Targa et al., 2022). During the offline sampling period (every second day), six samples exceeded 50 μg m^{-3}. While this sampling strategy does not allow a formal comparison with regulatory daily exceedance criteria- no more than 35 exceedances above 50

https://doi.org/10.5194/egusphere-2026-1708
Preprint. Discussion started: 10 August 2026

µg m^{-3} per year-the observed frequency is indicative of annual exceedance rate below the allowed limit and is lower than the average number of exceedance days reported for other sites in Serbia (Targa et al., 2022; SEPA, 2024).

Taken together, these observations suggest that PM_{10} levels at Ada Marina are consistent with compliance under the current EU and Serbian annual limit value framework (Fig. 4), although the sampling design does not permit a formal regulatory assessment. However, concentrations remain substantially above the updated WHO Air Quality Guideline of 15 µg m^{-3} (WHO, 2021). Furthermore, the revised EU Ambient Air Quality Directive introduces a stricter annual PM_{10} limit of 20 µg m^{-3} to be achieved by 2030 (European Parliament and Council, 2024). The present results therefore illustrate a clear gap between current legal thresholds and health-based guideline values, highlighting that sites meeting existing standards may still experience PM levels above those considered optimal for health protection.

Figure 4 shows that for Ada Marina, substantial reductions in anthropogenic sources, particularly residential wood burning in winter and fossil-fuel combustion year-round, would be required to move towards the WHO guideline and future EU limits. Organics in Fig. 4 are shown as OM, not OC, since the oxygen mass must be accounted for. OM/OC ratios used: BB = 1.8 (Levin et al., 2010) , FF = 1.2 (valid for hydocarbon-like organic aerosol, HOA, according to Zhang et al., 2005), PBAP = 2.1 (a representative central value from the literature, e.g., Heald and Spracklen, 2009), SOA = 2.0 (valid for oxygeated organic aerosol, OOA, Turpin and Lim, 2001; Zhang et al., 2005). Unapportioned PM_{10} in Fig. 4 is mainly accounted for by a mix of sulfate aerosol and mineral dust species (Petrović et al., in Prep.). Substantial contributions of RWC to PM_{10} are typical of the region, and similar findings have been reported across South-Eastern Europe where biomass burning is a dominant wintertime contributor to particulate pollution, including Athens (Theodosi et al., 2011), Sarajevo (Huremović et al., 2020), and other Balkan cities (Belis et al., 2013). Figure 4 also shows that EC_{BB}, and particularly OC_{BB}, represent major contributors to the PM burden especially if a substantial fraction of SOC is anthropogenic, and associated with RWC (discussed further in Sect. 3.3).

https://doi.org/10.5194/egusphere-2026-1708
Preprint. Discussion started: 10 August 2026

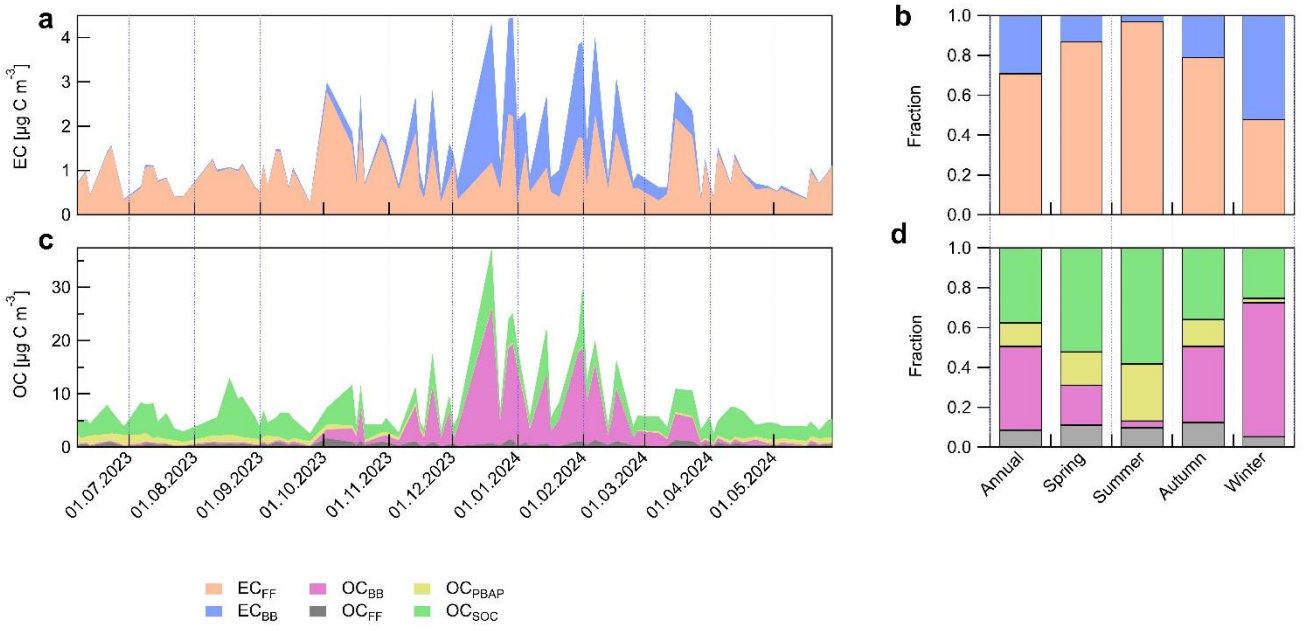

485 **Figure 3: (a, c) Time series of source-apportioned elemental carbon (EC) and organic carbon (OC) mass concentrations at the measurement site. In panel (a), orange shows EC from fossil fuel combustion (EC_{FF}) and blue shows EC from biomass burning (EC_{BB}). In panel (c), green shows total OC, with pink for OC from biomass burning (OC_{BB}), grey for OC from fossil fuel sources (OC_{FF}), yellow for OC from primary biological aerosol particles (OCPBAP), and bright green for secondary organic carbon (OC_{SOC}). (b, d) Seasonal averages of the fractional contributions to EC (b) and OC (d). Colours match panels (a, c), with stacked bars**
490 **indicating the seasonal share from fossil fuel (orange and grey), biomass burning (blue and pink), PBAP (yellow), and secondary organic aerosol (bright green) sources. OC shows strong biomass burning influence in winter and greater biogenic and secondary contributions in summer, while EC is consistently dominated by fossil fuel sources throughout the year.**

https://doi.org/10.5194/egusphere-2026-1708
Preprint. Discussion started: 10 August 2026

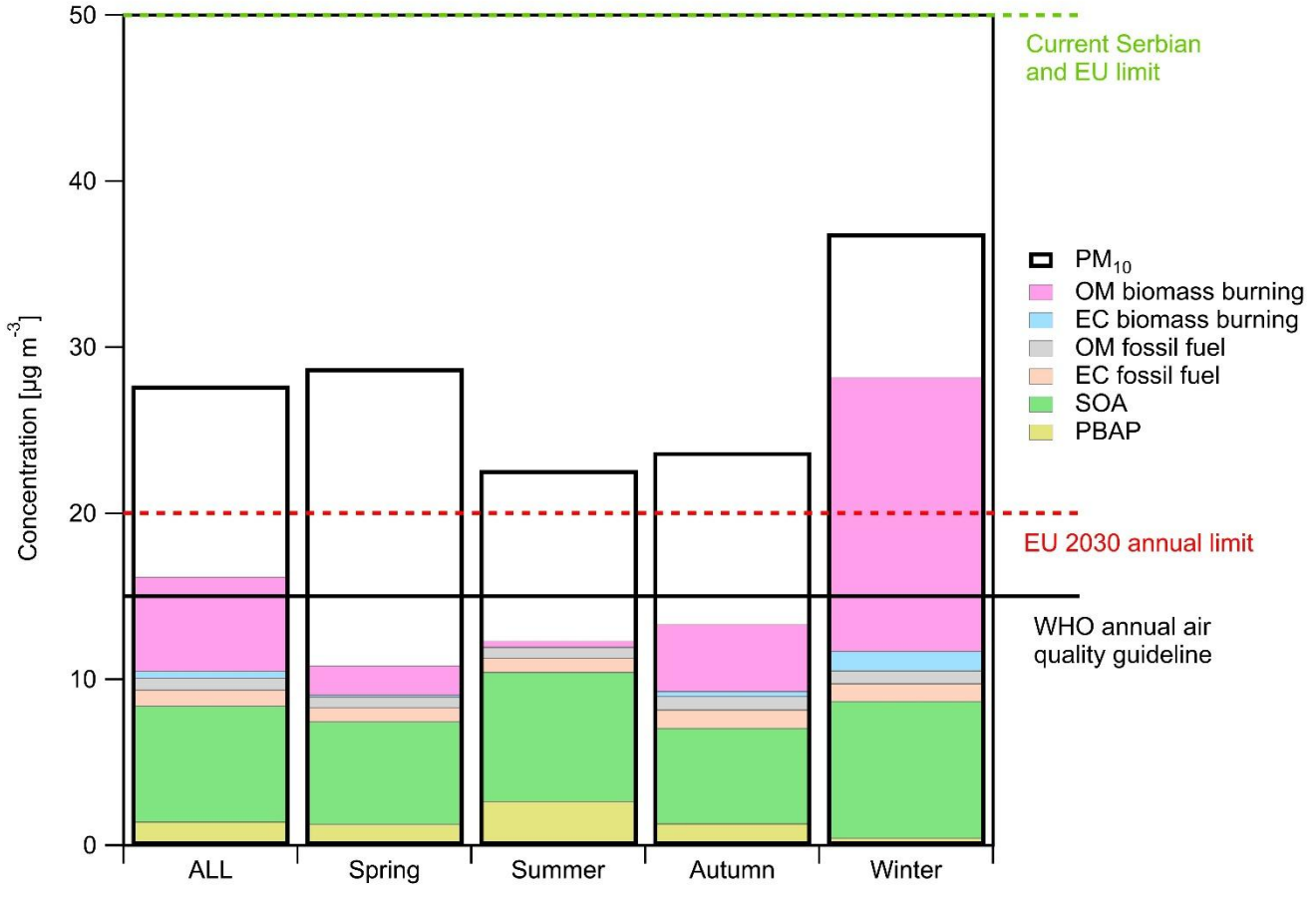

Figure 4: Seasonal and offline analysis period-average ("ALL") source apportionment of carbonaceous aerosol at Ada Marina. Stacked bars show organic matter (OM)—obtained by converting OC to OM using source-specific OM/OC and elemental carbon (EC). OM is partitioned into biomass burning (OM_{BB} fossil fuel (OM_{FF}), secondary organic aerosol (SOA; converted from SOC), and primary biological aerosol particles (PBAP). EC is split into EC_{BB} and EC_{FF}. Black outlines indicate measured PM_{10}. The green dashed line marks the current EU and Serbian annual limit for PM_{10} (50 µg m^{-3}); the red dashed line marks the EU AAQD 2030 PM_{10} annual limit (20 µg m^{-3}); the solid line marks the WHO PM_{10} annual guideline (15 µg m^{-3}).

Table 3: Annual offline analysis period and seasonal average concentrations of carbonaceous aerosol components, with uncertainty expressed as the standard deviation (in parentheses). Concentrations of organic carbon (OC) and elemental carbon (EC) are given in µg C m^{-3}, while other tracers (levoglucosan, arabitol, glucose, fructose, mannitol, trehalose, 2-methylerythritol) are reported in ng m^{-3}. Standard deviation for the measured values reflects observed variability. Calculated components include contributions from fossil fuel (FF), biomass burning (BB), primary biological aerosol particles (PBAP), and secondary organic carbon (SOC). Fractional contributions (fEC_{FF}, fEC_{BB}, fOC_{FF}, fOC_{BB}, fOC_{PBAP}, and fOC_{SOC}) represent each source's share of total EC or OC for the corresponding period. Contributions to PM_{10} are expressed as organic matter (OM). OM/OC used: BB = 1.8, FF = 1.2, PBAP = 2.1, SOA = 2.0, see main text.

	Annual	Spring	Summer	Autumn	Winter
Measured aerosol components					
PM_{10}	27.68 (16.61)	28.74 (19.28)	22.6 (9.50)	23.69 (6.32)	36.85 (23.95)

https://doi.org/10.5194/egusphere-2026-1708
Preprint. Discussion started: 10 August 2026

OC	8.12 (6.47)	5.39 (2.19)	6.28 (2.45)	6.62 (3.80)	14.2 (9.80)
EC	1.38 (1.03)	0.98 (0.62)	0.88 (0.34)	1.4 (0.84)	2.25 (1.41)
TC	9.5 (7.40)	6.37 (2.73)	7.16 (2.66)	8.02 (4.49)	16.45 (11.10)
Arabitol	34.84 (26.85)	33.66 (21.69)	62.45 (21.13)	34.48 (23.03)	8.79 (5.43)
Glucose	39.69 (25.93)	34.72 (14.66)	71.9 (23.94)	35.98 (13.52)	16.14 (10.40)
Fructose	10.16 (8.46)	11.97 (8.19)	18.17 (8.18)	8.14 (4.74)	2.37 (1.38)
Mannitol	39.5 (32.85)	31.84 (17.29)	80.4 (25.72)	37.58 (25.3)	8.2 (5.15)
Levoglucosan	412.99 (682.27)	129.32 (175.62)	28.52 (11.51)	294.92 (362.15)	1199.2 (930.75)
Trehalose	16.17 (11.51)	14.5 (6.94)	30.28 (11.46)	13.93 (5.72)	5.99 (3.40)
2-methylerythritol	5.01 (7.97)	1.46 (1.53)	14.6 (10.11)	3.76 (4.89)	0.23 (0.12)
2-methylthreitol	2.05 (2.78)	0.77 (0.65)	5.34 (3.36)	1.87 (1.95)	0.23 (0.13)
Calculated carbonaceous aerosol components					
EC_{FF}	0.83 (0.32)	0.7 (0.27)	0.84 (0.24)	1.01 (0.45)	1.01 (0.50)
EC_{BB}	0.09 (0.07)	0.08 (0.05)	0.03 (0.01)	0.16 (0.12)	0.9 (0.66)
OC_{FF}	0.51 (0.21)	0.43 (0.17)	0.51 (0.15)	0.62 (0.28)	0.6 (0.29)
OC_{BB}	0.69 (0.54)	0.6 (0.38)	0.21 (0.06)	1.27 (0.89)	7.01 (5.12)
OC_{PBAP}	0.8 (0.45)	0.67 (0.33)	1.57 (0.27)	0.81 (0.12)	0.24 (0.12)
OC_{SOC}	2.75 (1.05)	2.65 (0.57)	3.08 (1.35)	2.68 (1.44)	3.29 (1.33)
Fractional contributions to EC					
fEC_{FF}	0.79 (0.21)	0.88 (0.12)	0.97 (0.01)	0.81 (0.16)	0.52 (0.18)
fEC_{BB}	0.21 (0.21)	0.12 (0.12)	0.03 (0.01)	0.19 (0.16)	0.48 (0.18)
Fractional contributions to OC					
fOC_{FF}	0.09 (0.04)	0.1 (0.04)	0.09 (0.03)	0.11 (0.06)	0.06 (0.04)
fOC_{BB}	0.27 (0.25)	0.16 (0.14)	0.04 (0.01)	0.29 (0.22)	0.59 (0.14)
fOC_{PBAP}	0.16 (0.14)	0.17 (0.10)	0.29 (0.13)	0.16 (0.11)	0.03 (0.02)
fOC_{SOC}	0.48 (0.17)	0.58 (0.12)	0.58 (0.13)	0.44 (0.18)	0.33 (0.11)
Fractional contributions to PM_{10}					
fEC_{FF}	0.05 (0.03)	0.05 (0.04)	0.04 (0.02)	0.06 (0.03)	0.04 (0.03)
fEC_{BB}	0.02 (0.02)	0.01 (0.01)	0.00 (0.00)	0.02 (0.02)	0.04 (0.02)
fOM_{FF}	0.03 (0.02)	0.04 (0.03)	0.03 (0.01)	0.04 (0.02)	0.03 (0.02)
fOM_{BB}	0.22 (0.31)	0.09 (0.10)	0.02 (0.01)	0.23 (0.29)	0.56 (0.32)
fOM_{PBAP}	0.11 (0.11)	0.12 (0.14)	0.18 (0.09)	0.09 (0.07)	0.03 (0.03)
fOM_{SOA}	0.32 (0.15)	0.37 (0.20)	0.35 (0.18)	0.32 (0.12)	0.26 (0.08)

https://doi.org/10.5194/egusphere-2026-1708
Preprint. Discussion started: 10 August 2026

3.2 Equivalent black carbon and its optical properties

The mean eBC concentration at Ada Marina for the online analysis period was 1.42±1.40 μg m^{-3} (Table 4), slightly higher than the median and median absolute deviation, 0.9±0.48 μg m^{-3}, reflecting a skewed distribution due to a few high concentration episodes, particularly in the wintertime (Fig. 5a). Mean eBC is similar to other urban background sites across Europe, for example 1.3±1.4 μg m^{-3} from a dataset including 23 urban background sites (Savadkoohi et al., 2023). Although there are few eBC measurements for South-Eastern Europe, our values are broadly consistent with, though slightly lower than, observed elsewhere. For example Diapouli et al. (2017) report eBC concentrations of 2.4±1.0 μg m^{-3} and 1.6±0.6 μg m^{-3}, during cold and warm periods, respectively, in Athens, Greece, in 2013 to 2014. Meanwhile Savadkoohi et al. (2023) find mean eBC of 1.76±2.2 μg m^{-3} in Athens, for 2017 to 2019. However, these higher levels may be reflective of the decreasing trend in eBC seen more broadly across Europe (Savadkoohi et al., 2023), when compared to the more recent time series of this study. Masić (2024) presented somewhat higher eBC levels for Sarajevo (2.94 μg m^{-3}) and Zenica (2.06 μg m^{-3}), both located in Bosnia Herzegovina for years 2022 to 2023. The elevated levels observed at those sites likely reflect more persistent wintertime pollution episodes, local emission sources, and topographical conditions that exacerbate atmospheric stagnation. Ćirović et al. (2025) found even higher eBC levels in Belgrade city centre during winter in 2020 of eBC = 4.43 μg m^{-3}. The data presented here spans a full year and thus fill a critical gap in the region's observational record. In summary, unlike for PM_{10}, Ada Marina represents a moderately polluted urban-background site within a European context and a low polluted site within Southeastern Europe.

Seasonal variability at the Ada Marina site is strong, with lower concentrations in summer compared to winter. We observed a peak monthly mean of 2.67 μg m^{-3} in December 2024, compared to 0.72 μg m^{-3} in May 2025. Higher winter concentrations are typical, and due to the presence of eBC from RWC during colder months, as described in numerous previous studies (e.g., Caseiro et al., 2009; Sandradewi et al., 2008a; Favez et al., 2010). Diurnal profiles are also typical (Fig. 5b), with elevated levels seen in the morning and in the evening due to traffic patterns and RWC in the evenings. Interestingly, the morning peak occurs approximately one hour later in winter (~08:00 UTC, or 09:00 local time) compared to summer (~06:00 UTC, or 08:00 local time), while the evening peak occurs earlier in winter (~20:00 UTC, 21:00 local time) compared to summer (~21:00 UTC, or 22:00 local time). This pattern likely reflects the shorter daylight hours in winter with people leaving home later and returning earlier, with reduced outdoor and commercial activity after sunset.

As Fig. 5c shows, there is also a distinct seasonal variability in optical properties, not only concentrations. The mean AAE is 1.54 in winter and 1.18 in summer (Table 4), which closely follows the overall trend in eBC, though the minimum occurs slightly later (July rather than May). This coincides with wintertime elevated brown carbon fractions (f_{BrC}) of 0.44 ± 0.11 (Table 4), indicating a seasonal shift from BrC-rich biomass combustion sources in winter to more fossil fuel–dominated emissions in summer. These differences are consistent with numerous established studies across Europe and Asia, where higher

https://doi.org/10.5194/egusphere-2026-1708
Preprint. Discussion started: 10 August 2026

winter AAE values are attributed to RWC and coal combustion, both rich in BrC (e.g., Popovicheva et al., 2022; Savadkoohi et al., 2023; Wang et al., 2018).

The diurnal cycle of the AAE is also different in winter and summer, with a distinct pattern of higher AAE overnight seen in winter, but not in summer. While AAE is theoretically independent of concentration, the observed diurnal pattern in winter likely reflects boundary-layer-driven shifts in the composition and source contributions of absorbing aerosols. Shallow layers in the morning and evening can trap fresh biomass burning emissions rich in brown carbon, raising AAE, whereas a deeper, well-mixed boundary layer during summer homogenises aerosol composition and suppresses diurnal variability (Liu et al., 2023; Jiang et al., 2025).

Figure 6 further supports the seasonal interpretation of BrC influence at Ada Marina by comparing observed versus extrapolated absorption spectra. In panel (a), representing summer, the measured absorption coefficients (B_{ABS} observed, blue) closely follow the extrapolated curve derived from a power-law fit to the 520 to 950 nm range (B_{ABS} expected, black), with little enhancement at shorter wavelengths. This spectral consistency suggests dominance of black carbon (BC) from fossil fuel combustion with negligible contribution from BrC, consistent with the low f_{BrC} (0.12 ± 0.06) and low AAE (1.18 ± 0.06) reported in Table 4 for summer.

In contrast, Fig. 6 panel (b) shows winter conditions, where observed absorption at shorter wavelengths (especially 370 nm and 470 nm) clearly exceeds the power-law extrapolation from longer wavelengths. This spectral enhancement is characteristic of BrC absorption, which selectively enhances in the UV to visible range. This agrees with the higher f_{BrC} (0.44 ± 0.11) and AAE (1.54 ± 0.14) observed during winter, and with the diurnal pattern in AAE (Fig. 5d) suggesting temporally varying BrC contributions. The mismatch between observed and extrapolated B_{Abs} in winter also highlights that power-law assumptions are violated, especially under strong BrC influence. This implies that bulk AAE values derived from full-spectrum fits may be biased, and source apportionment models that assume strict power-law behavior (e.g., the classic aethalometer model) should

https://doi.org/10.5194/egusphere-2026-1708
Preprint. Discussion started: 10 August 2026

be applied with care, especially during winter, episodic biomass burning events, or when BrC is strong or when designing targeted mitigation measures.

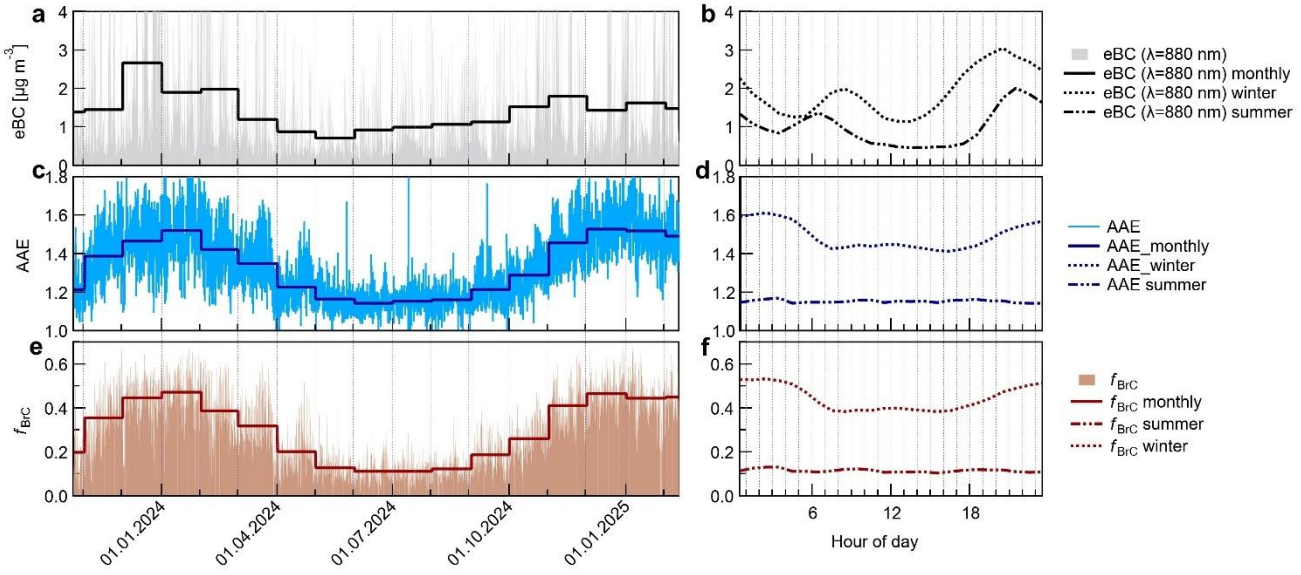

Figure 5: Temporal and diurnal variability of equivalent black carbon at λ=880 nm (eBC), the absorption Ångström exponent (AAE), and the brown carbon fraction (f_{BrC}) at λ=370 nm. (a) Time series of eBC derived from absorption at λ=880 nm (grey), with superimposed monthly averages (solid black). (b) Diurnal cycle of eBC, showing monthly (solid), winter (dashed), and summer (dash-dotted) averages. (c) AAE computed from fitted (log B_{Abs} vs log wavelength) absorption at λ=520 to 950 nm (light blue), with monthly, winter, and summer averages shown in bold dark blue lines. (d) Time series of the fractional contribution of brown carbon (f_{BrC}) to total absorption at λ=370 nm, calculated using the subtraction method. Here, brown carbon absorption is estimated as the difference between total absorption and a black carbon contribution extrapolated from 880 nm using a fixed AAE of 1. (f) Diurnal variation of f_{BrC}, showing monthly, winter, and summer means. The time zone is UTC.

https://doi.org/10.5194/egusphere-2026-1708
Preprint. Discussion started: 10 August 2026

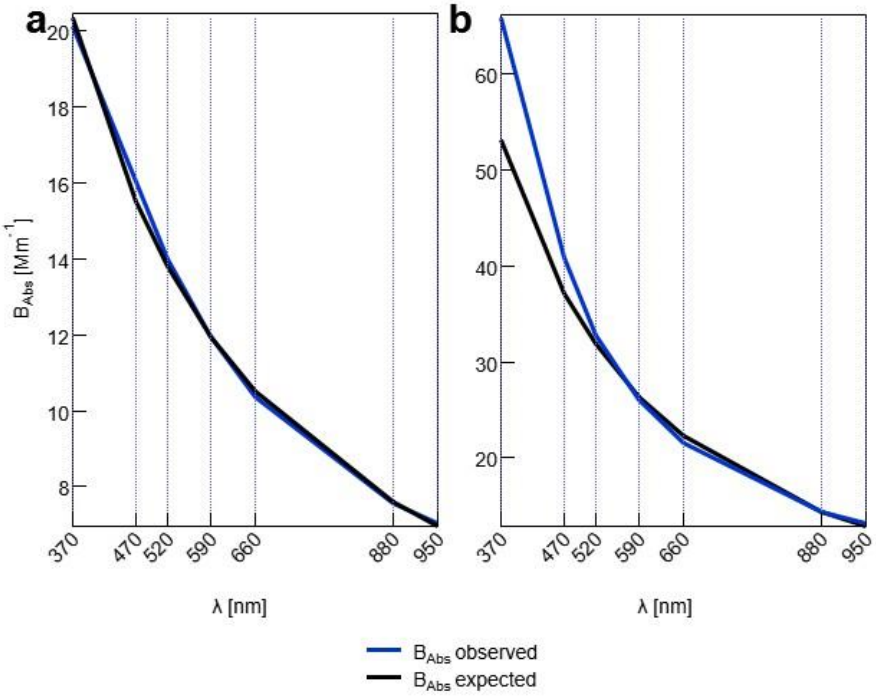

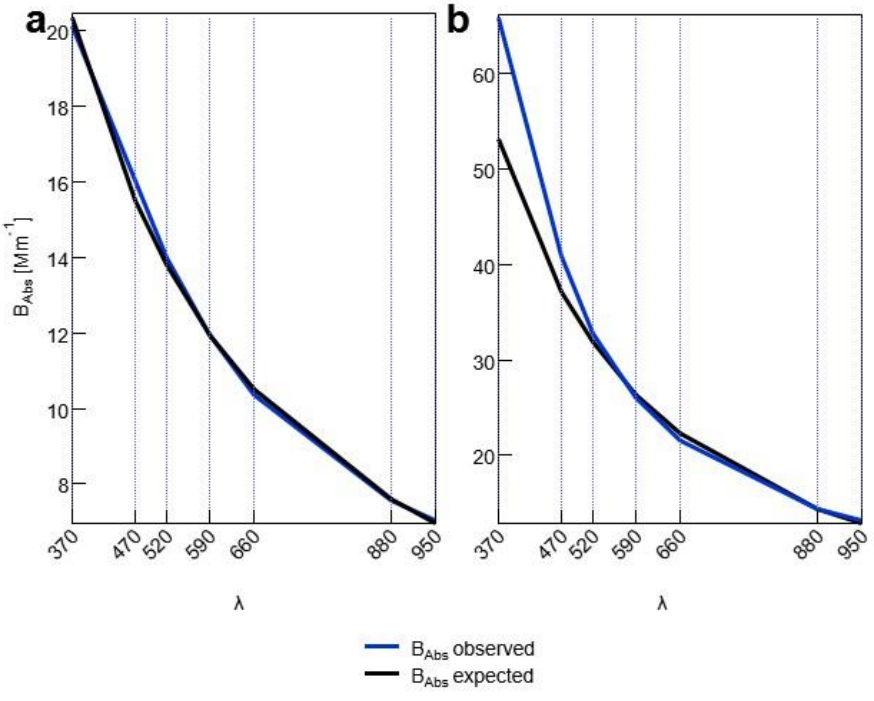

https://doi.org/10.5194/egusphere-2026-1708
Preprint. Discussion started: 10 August 2026

Figure 6: Observed and extrapolated B_{ABS} spectra. Average observed absorption coefficients (B_{ABS} observed, blue) and expected values (B_{ABS} expected, black) based on extrapolation from 880 nm, using a log–log linear fit to data at 520 to 950 nm, assuming power-law behaviour (Eq. 1). Panel (a) shows summer data with relatively low BrC influence; panel (b) shows stronger short-wavelength absorption indicative of enhanced BrC in winter.

Table 4: Seasonal and overlapping-period (concurrent optical and filter analyses in the period 23 October 2023 to 29 May 2024, (Fig. 1) means and standard deviation (in parentheses) for equivalent black carbon (eBC), the fractional contribution of brown carbon determined at 370 nm (f_{BrC}), and the bulk absorption Ångström exponent (AAE) from the aethalometer measurements, and elemental carbon (EC) from the offline analysis.

Component	Online measurement period	Spring	Summer	Autumn	Winter	Overlapping period
eBC [μg m^{-3}]	1.42 (1.40)	0.93 (0.89)	1.00 (0.81)	1.47 (1.33)	1.9 (1.76)	1.63 (1.35)
f_{BrC}	0.29 (0.17)	0.22 (0.12)	0.12 (0.06)	0.3 (0.13)	0.44 (0.11)	0.32 (0.14)
AAE	1.37 (0.19)	1.28 (0.13)	1.18 (0.06)	1.37 (0.15)	1.54 (0.14)	1.40 (0.15)
EC						1.60 (1.19)

3.3 Source apportionment of online data

Following the approach of Savadkoohi et al. (2025), we derived AAE at the first percentile (P1) = 1.02 (for summer bulk B_{Abs} data) and 99th percentile (P99) = 1.81 (for full period bulk B_{Abs} data) for use in the aethalometer model (Fig. 7). These AAE values are consistent with the literature for liquid (AAE_{LF}) and solid (AAE_{SF}) fuel burning sources. For example, Savadkoohi et al. (2025), find P1 values of between 0.94 and 1.11 for urban sites and 0.98 for a traffic dominated site (Helsinki-Mäkelänkatu), and P99 values (winter) of between 1.46 and 1.72 for urban sites and 1.45 for Helsinki-Mäkelänkatu. Savadkoohi et al. (2025) also note that, for traffic dominated sites, P99 likely provides a lower-bound estimate of AAE_{SF}, as the true AAE for solid fuels is expected to be higher, since a large fraction of LF sources is likely always present. This is further shown by the bimodal distribution of the bulk AAE data, which is driven by a marked separation in winter and summer optical properties (Fig. 7). As shown in Table 5, using these AAE values and the aethalometer model we find good agreement between eBC_{LF} and EC_{FF} (Pearson's R^2=0.89) and eBC_{SF} and EC_{BB} (Pearson's R^2 = 0.99). We also show that the latter extremely high correlation is not a statistical artefact driven by high seasonal variability in solid fuel burning (i.e., very low in summer, very high in winter, driving strong correlation) since it remains high when considering the overlapping winter period only (Pearson's R^2 = 0.99).

Furthermore, only a small fraction of negative source contributions from SF or LF (1.6%) was observed, indicating generally stable behaviour of the model under the chosen parameterisation. However, this should not be interpreted as strict validation of the assumed a priori AAEs. In the aethalometer model, the use of single AAE values for solid and liquid fuel sources implicitly assumes that the true distributions of combustion-related AAEs are centred on these constant values. In reality, AAE varies substantially with combustion conditions, fuel type, mixing state, and atmospheric processing. As a result, for example,

https://doi.org/10.5194/egusphere-2026-1708
Preprint. Discussion started: 10 August 2026

some strong biomass-burning events may exhibit ambient AAEs higher than the fixed AAE_{SF} used in the model. In such cases, the model can produce apparent solid-fuel contributions exceeding 100% of total BC. The low occurrence of negative contributions therefore suggests that the selected AAEs, while producing internally consistent solutions for most conditions are too low to represent e.g., episodes of high concentrations from solid fuel eBC.

AAE values derived from NNMF are emergent rather than prescribed. Nevertheless, the weight matrix H (factor spectral profiles; purple lines in Fig. 8) closely follows the physically expected power-law behaviour of B_{ABS}(black lines in Fig. 8). This indicates that NNMF provides a physically meaningful representation of the aethalometer absorption spectra. The results presented here are based on an ensemble of 500 NNMF runs. Ensemble variability, rotational ambiguity, and goodness-of-fit diagnostics (residual distributions) are evaluated in Fig. S4. The same diagnostics are shown for a three-factor solution in Fig. S5, which was rejected due to instability and lack of well-resolved factors.

The emergent AAEs from NNMF are similar to, but slightly higher than, those obtained using the percentile-based approach ($AAE_{LF} = 1.17$, $AAE_{SF} = 1.86$ versus $AAE_{LF} = 1.02$ and $AAE_{SF} = 1.81$). This supports the argument above that the a priori AAEs used in the aethalometer model may be somewhat low, particularly for strong biomass-burning episodes. Using NNMF derived AAEs in the aethalometer model increases the fraction of negative points from 1.6% (using AAEs derived from the bulk distribution) to 14%. Interestingly, the NNMF-derived AAE_{LF} approximates the mode of the summertime AAE distribution (Fig. 7), when biomass-burning influence is minimal according to the offline tracer analysis. In contrast, the NNMF-derived AAE_{SF} lies near the upper edge of the bulk AAE distribution, above P99.

Strict adherence to a power-law dependence is not necessarily advantageous, especially in the presence of brown carbon (BrC), and similar deviations are evident in the bulk absorption spectra (Fig. 6). BrC enhances absorption at shorter wavelengths (Lack and Cappa, 2010), causing $B_{\mathrm{Abs}}$to deviate from idealised power-law behaviour. Under such conditions, the aethalometer model may overestimate BC concentrations (Kirchstetter et al., 2004). The ability of NNMF to capture these spectral deviations without imposing rigid functional assumptions therefore represents a key methodological advantage (Fig. 8).

Figure 8 also shows that enhanced absorption at lower wavelengths is associated with the solid fuel factor. This is expected, as fuel-rich combustion conditions favor BrC formation (Laskin et al., 2015), while fossil fuel combustion, such as from diesel engines, generally produces only modest amounts of BrC (Liu et al., 2015). However, the chemistry of brown carbon is complex, with its abundance and optical properties controlled by competing processes, including atmospheric aging and the molecular composition of BrC species. Typically, aging leads to a decrease in BrC due to photochemical bleaching and oxidation, especially in biomass burning plumes, as chromophores degrade over time (Forrister et al., 2015). Low molecular weight BrC compounds, such as nitrophenols, can photobleach within hours, whereas high molecular weight BrC species are more stable (Wong et al., 2019). Conversely, initial atmospheric aging can lead to the formation of secondary BrC, temporarily enhancing absorption (Gilardoni et al., 2016; Kalbermatter et al., 2022).

At Ada Marina, we observe a relatively high correlation between the solid fuel factor and secondary organic carbon (SOC), with $R^2 = 0.76$ increasing to 0.86 in winter for NNMF, and 0.74 increasing to 0.84 for the aethalometer model. This consistent association between solid fuel BC and SOC, enhanced absorption at lower wavelengths in the NNMF solid fuel factor,

https://doi.org/10.5194/egusphere-2026-1708
Preprint. Discussion started: 10 August 2026

combined with the proximity to urban areas such as Čukarička Padina and Banovo Brdo at the right bank and New Belgrade at the left bank of the Sava, suggests that local emissions are primarily responsible for both BrC and a significant fraction of SOC via initial aging leading to temporarily enhanced absorption.

Overall, the NNMF and aethalometer model approaches yield very similar results with respect to correlation to offline analyses (Table 5), and a clear diurnal pattern for both solid and liquid fuel factors (solid fuel peaking overnight and liquid fuel peaking during the morning and early evening during expected peak traffic, Fig. 9b,d,f). Notably however, the NNMF approach yields stronger annual and diurnal variability for the solid fuel factor, with monthly average levels peaking slightly higher in December 2023 (1.65 vs 1.64 μg m^{-3} according to the aethalometer model, Fig. 9c) and significantly lower than the aethalometer model average of 0.16 μg m^{-3} in summer, at 0.05 μg m^{-3} (Table 4). This stronger seasonal variation is supported by analysis of offline data, where average levoglucosan derived EC_{BB} is also 0.03 μg m^{-3} in summer (Table 3), though noting that the summertime periods do not overlap. Diurnal variation is also slightly more distinct for the solid fuel fraction in NNMF, since the aethalometer model approach has a slight morning peak around 7 to 8 AM UTC (Fig. 9d).

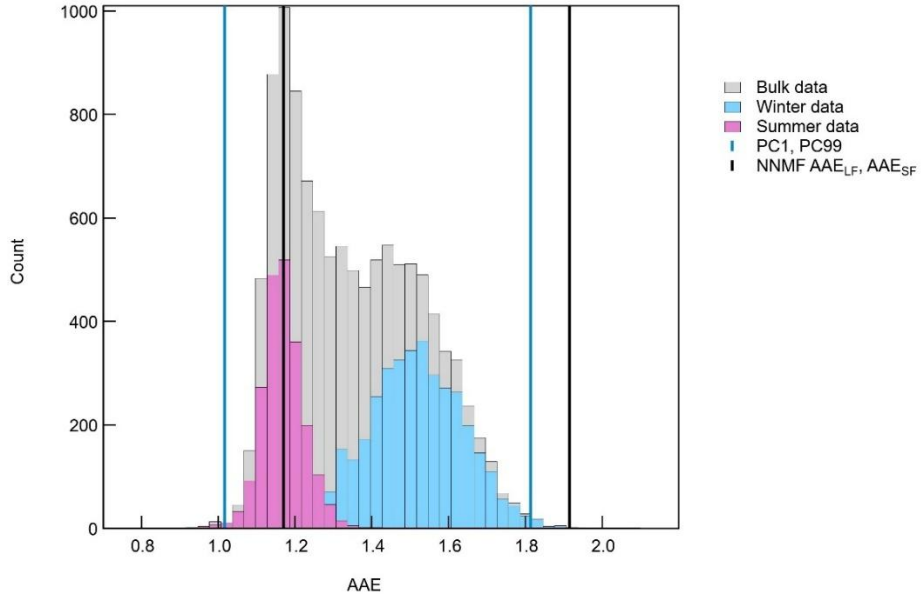

Figure 7: Histograms of absorption Ångström exponents (AAE) derived from the slope of log(absorption) versus log(wavelength), based on the full dataset (grey), and for winter (blue) and summer (magenta subsets. Vertical blue lines indicate the 1st (PC1) and 99th (PC99) percentiles used in the optimized aethalometer model, as well as emergent AAEs derived from non-negative matrix factorization (NNMF) liquid fuel (LF) and solid fuel (SF) factors.

https://doi.org/10.5194/egusphere-2026-1708
Preprint. Discussion started: 10 August 2026

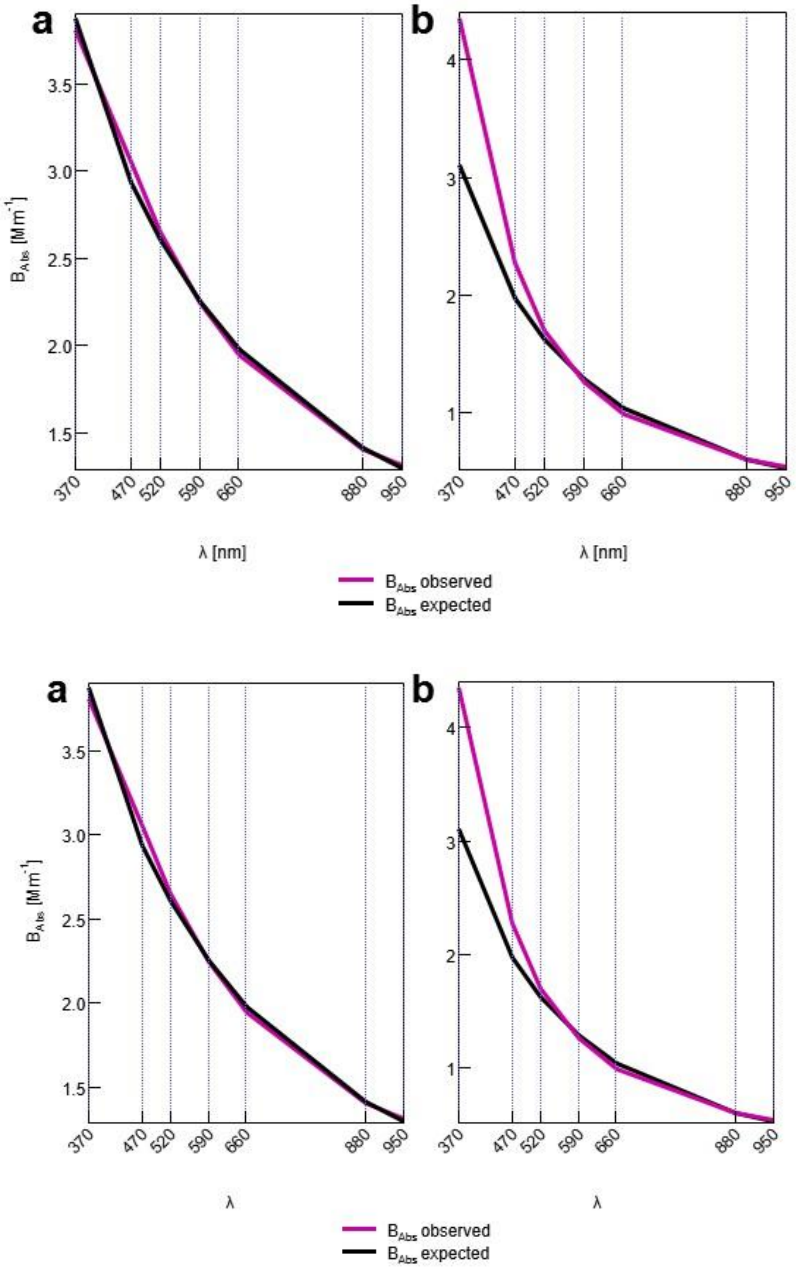

655

Figure 8: Observed and extrapolated B_{ABS} spectra. Average observed absorption coefficients (B_{ABS} observed, purple) and expected values (B_{ABS} expected, black) based on extrapolation from 880 nm, using a log–log linear fit to data at 520 to 950 nm, assuming power-law behaviour (Eq. 1) from NNMF. Panel (a) shows NNMF factor 1 (liquid fuel) with low BrC influence; panel (b) shows stronger short-wavelength absorption indicative of enhanced BrC in factor 2 (solid fuel).

660

https://doi.org/10.5194/egusphere-2026-1708
Preprint. Discussion started: 10 August 2026

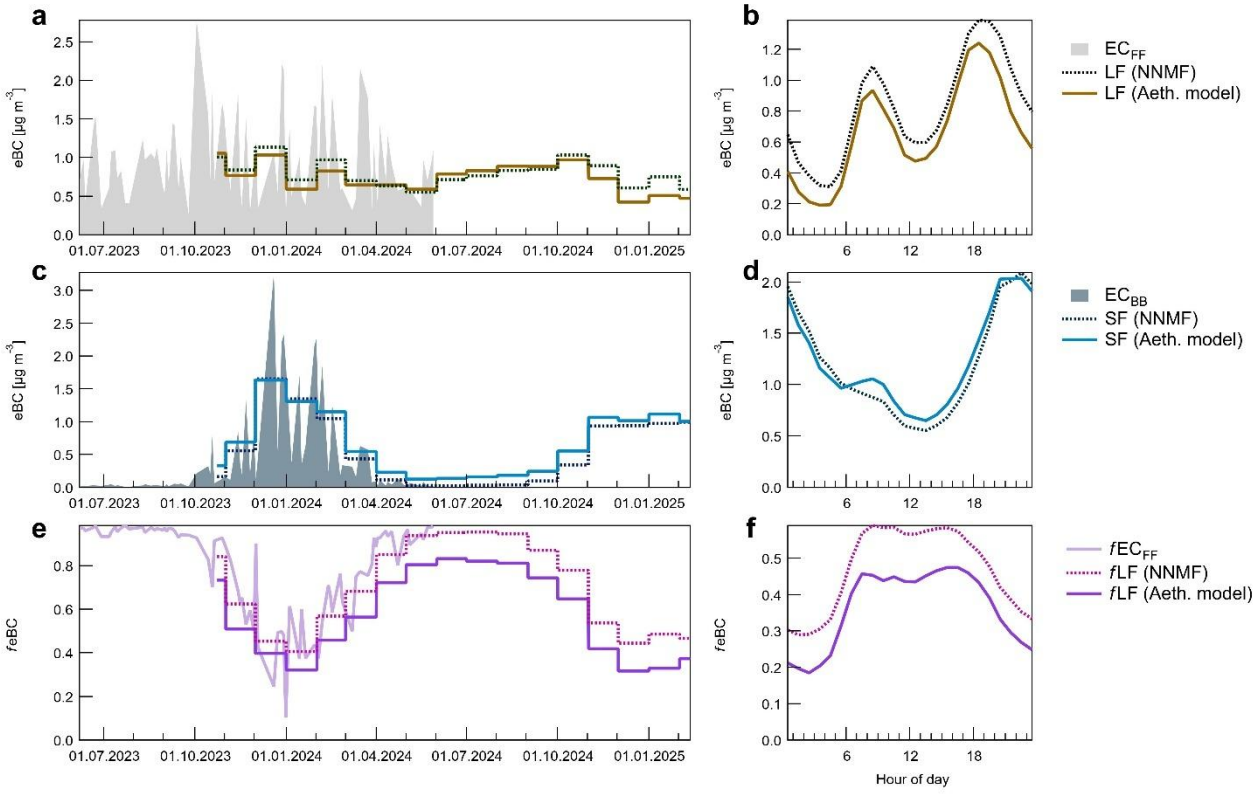

Figure 9: Seasonal and diurnal variation in equivalent black carbon (eBC) concentrations and source contributions at Ada Marina, based on offline and online source apportionment methods. (a, c, e) Monthly average eBC apportioned to liquid fuel (LF, panel a) and solid fuel (SF, panel c) sources from the aethalometer model (solid lines) and NNMF (dashed lines), shown alongside offline EC-based estimates for EC from fossil fuel (EC_{FF}) and biomass burning (EC_{BB}, shaded areas). The aethalometer model uses the 520 nm to 880 nm wavelength pair. Panel (e) shows the corresponding fraction of liquid fuel-derived eBC (f_{LF}) or EC (EC_{FF}) from all three approaches. (b, d, f) Diurnal patterns of eBC from liquid fuel (b), solid fuel (d), and the fractional contribution of fossil fuel or LF (f) during winter. Solid lines represent the aethalometer model, and dashed lines indicate NNMF results.

Table 5: Seasonal and overlapping-period statistics for equivalent black carbon from fossil fuel (LF) and solid fuel (SF) sources, derived using the aethalometer model (using the 520 to 880 nm wavelength range), NNMF, and compared with source-apportioned elemental carbon (EC) from offline filter analyses.. All values represent the median (median absolute deviation, MAD). The upper rows show concentrations of LF and SF (µg m^{-3}) and their fractional contributions (fLF, fSF) to total eBC. The lower rows list coefficients of determination (R^2) between aethalometer-derived and calculated apportioned EC from fossil fuel (EC_{FF}), EC from biomass burning (EC_{BB}), OC from fossil fuel (OC_{FF}), OC from biomass burning (OC_{BB}), and OC from secondary organic carbon (OC_{SOC}) during the overlapping measurement period (concurrent optical and filter analyses in the period 23 October 2023 to 29 May 2024, Fig. 1).

Component	Aethalometer measurement period	Spring	Summer	Autumn	Winter	Overlapping period
			Aethalometer model			
LF [µg m^{-3}]	0.74 (0.77)	0.63 (0.6)	0.84 (0.73)	0.85 (0.81)	0.66 (0.82)	0.75 (0.46)
SF [µg m^{-3}]	0.67 (0.94)	0.3 (0.43)	0.16 (0.14)	0.62 (0.75)	1.23 (1.23)	0.87 (1.00)

https://doi.org/10.5194/egusphere-2026-1708
Preprint. Discussion started: 10 August 2026

f_{LF}	0.58 (0.24)	0.7 (0.16)	0.82 (0.07)	0.59 (0.19)	0.36 (0.2)	0.55 (0.19)
f_{SF}	0.42 (0.24)	0.3 (0.16)	0.18 (0.07)	0.41 (0.19)	0.64 (0.2)	0.45 (0.19)
			NNMF			
LF [μg m^{-3}]	0.83 (0.79)	0.65 (0.6)	0.78 (0.63)	0.95 (0.85)	0.86 (0.9)	0.85 (0.54)
SF [μg m^{-3}]	0.56 (0.96)	0.19 (0.4)	0.05 (0.04)	0.45 (0.69)	1.15 (1.28)	0.8 (1.04)
f_{LF}	0.71 (0.25)	0.83 (0.16)	0.94 (0.04)	0.73 (0.2)	0.49 (0.21)	0.67 (0.21)
f_{SF}	0.29 (0.25)	0.17 (0.16)	0.06 (0.04)	0.27 (0.2)	0.51 (0.21)	0.33 (0.21)
			Offline source apportionment			
fEC$_{FF}$						0.70 (0.22)
fEC$_{BB}$						0.30 (0.22)

Table 6: Pearson correlation coefficients between source apportionment components from the aethalometer model and NNMF, as well as offline tracer-derived proxies, for the full overlapping period (top) and winter only (bottom). The table includes correlations between liquid fuel (LF) and solid fuel (SF) sources (highlighted red) estimated from the aethalometer model (using the 520 to 880 nm wavelength pair) and NNMF, and offline-derived EC, OC, and secondary organic carbon (SOC) components. High correlations between SF and SOC (especially in winter, highlighted green) suggest potential interference from SOC coating on particles, affecting the aethalometer-derived source estimates.

Full overlapping period

	Aethalometer model							NNMF						
	LF	SF	EC$_{FF}$	EC$_{BB}$	OC$_{FF}$	OC$_{BB}$	SOC	LF	SF	EC$_{FF}$	EC$_{BB}$	OC$_{FF}$	OC$_{BB}$	SOC
LF	1.00	0.68	0.89	0.64	0.89	0.64	0.46	1.00	0.75	0.87	0.77	0.87	0.77	0.53
SF		1.00	0.53	0.99	0.51	0.99	0.74		1.00	0.47	0.99	0.45	0.99	0.76
EC$_{FF}$			1.00	0.41	1.00	0.41	0.36			1.00	0.41	1.00	0.41	0.36
EC$_{BB}$				1.00	0.38	1.00	0.48				1.00	0.38	1.00	0.48
OC$_{FF}$					1.00	0.38	0.35					1.00	0.38	0.35
OC$_{BB}$						1.00	0.48						1.00	0.48
SOC							1.00							1.00

Winter overlapping period

	Aethalometer model							NNMF						
	LF	SF	EC$_{FF}$	EC$_{BB}$	OC$_{FF}$	OC$_{BB}$	SOC	LF	SF	EC$_{FF}$	EC$_{BB}$	OC$_{FF}$	OC$_{BB}$	SOC
LF	1.00	0.78	0.83	0.77	0.83	0.77	0.47	1.00	0.80	0.85	0.83	0.84	0.83	0.54
SF		1.00	0.60	0.99	0.59	0.99	0.84		1.00	0.54	0.98	0.52	0.98	0.86
EC$_{FF}$			1.00	0.58	1.00	0.58	0.35			1.00	0.58	1.00	0.58	0.35
EC$_{BB}$				1.00	0.57	1.00	0.78				1.00	0.57	1.00	0.78
OC$_{FF}$					1.00	0.57	0.34					1.00	0.57	0.34

https://doi.org/10.5194/egusphere-2026-1708
Preprint. Discussion started: 10 August 2026

OC_{BB}		1.00	0.78		1.00	0.78
SOC			1.00			1.00

3.4 Atmospheric transport

Figure 10 a to c shows footprint emissions sensitivities (FES) at Ada Marina. Warm colours mean the air arriving at the site spent more time close to the surface over those locations (higher sensitivity to emissions). FES depends on meteorology and removal only; it does not include emissions. To infer likely source regions, we combined the FES with gridded emissions to create emission weighted footprint, EWF (FES × emissions), combining atmospheric sensitivity with where emissions occur (Fig. 10 d to f). During the colder months, November to March, Ada Marina is more sensitive to emissions from a slightly broader region. This is exemplified by episodes of sustained high eBC concentrations associated with northerly transport over the Pannonian Basin (from Croatia, Austria, and the Czech Republic) alongside locally high footprint sensitivity at Ada Marina (Fig. 11), As Fig. 11 also shows, the lowest levels during colder months are associated mainly with sensitivity to North Easterly regions (Poland, Moldova, Ukraine, and Russia).

As described in Sect. 2.4, modelled BC from the gridded inventory is partitioned into various sectors. Because the observational groupings, offline tracer–derived EC_{BB} and residual EC_{FF}, and NNMF-derived liquid and solid eBC factors, do not map one-to-one onto these inventory categories, we systematically paired each source-apportioned factor with all combinations of model categories to find the highest overall Pearson's R^2. Across both the offline tracer and NNMF evaluations, the residential (i.e., cooking and heating) vs. non-residential (i.e., all other model emissions) split of the modelled emissions yielded the highest overall correlation with SA results.

Figure 12 summarises the agreement for three pairings: residential vs. EC_{BB} and NNMF eBC_{SF}, non-residential vs. EC_{FF} and NNMF eBC_{LF}, and total modelled BC vs. EC and eBC. Residential vs. EC_{BB} and residential vs. eBC_{SF} have higher R^2 with standard deviation (σ)-ratios near unity, indicating that the site captures the model residential-heating signal cleanly. Non-residential vs. EC_{FF} and eBC_{LF} shows respectable correlation but tends toward under-dispersion (σ-ratio < 1), consistent with a modest underestimation of near-road variability, reflecting the proximity of Ada Marina to major roads (Fig. 2). Including the Fire BC category (wildfires, agricultural burning) with the residential emissions and excluding it from the non-residential category did not improve agreement with EC_{BB} and eBC_{SF}. This suggests only a minor contribution at this site and period, or poor temporal alignment with the filter sampling. As expected, total BC vs EC/eBC performs worse than the targeted pairings (though still agreeing very well), reinforcing that evaluation is most interpretable when model categories are aligned with residential vs. non-residential source influence. Overall, the Taylor analysis shows that the residential heating component is both influential and well constrained at Ada Marina. This supports the source apportionment results and indicates that residential emissions represent a substantial and diagnostically robust contributor to BC at the site. The strong model–measurement agreement further suggests that emission changes in this sector would likely produce detectable responses in the carbonaceous aerosol burden, enabling prospective scenario analysis and retrospective evaluation of emission trends.

https://doi.org/10.5194/egusphere-2026-1708
Preprint. Discussion started: 10 August 2026

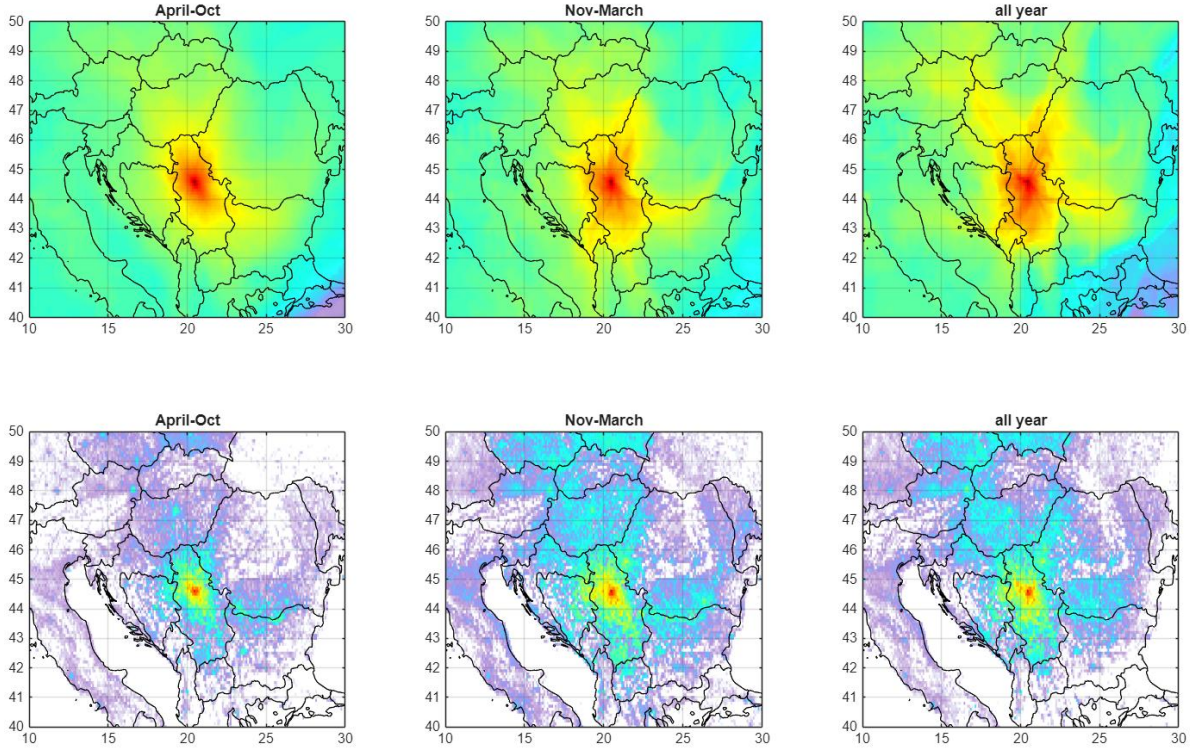

Figure 10: Seasonal footprint emission sensitivity (FES) from FLEXPART for the Ada Marina receptor, using 21-day backward simulations with a BC tracer including dry/wet deposition, turbulence, unresolved mesoscale motions, and deep convection. Panels a to c (top): mean FES for April to October (in years 2023 and 2024), November–March (in years 2023, 2024), and all year. Panels d to f (bottom): corresponding emission-weighted footprints (footprint × gridded BC emissions), representing the modelled spatial contribution of BC emissions to concentrations at Ada Marina for the same periods.

https://doi.org/10.5194/egusphere-2026-1708
Preprint. Discussion started: 10 August 2026

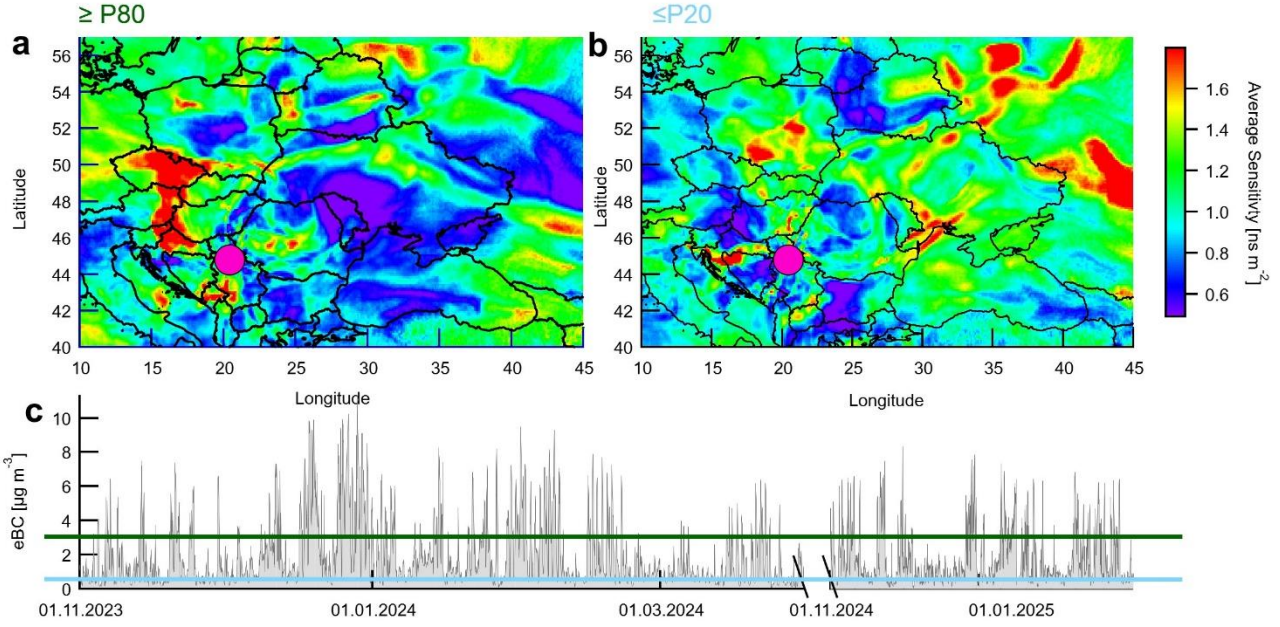

Figure 11: Footprint emission sensitivities and eBC time series for Ada Marina. (a) Mean footprint emission sensitivity for hours when eBC ≥ P80 (top 20% of the concentration distribution). (b) Same for eBC ≤ P20 (bottom 20%). The magenta circle marks the receptor (Ada Marina). Colours show the average sensitivity in ns m⁻², where larger values indicate longer residence time of air parcels over the surface and hence a greater sensitivity to emissions in those grid cells. c) time series of eBC at Ada Marina during November to March 2023 and November to February 2024.

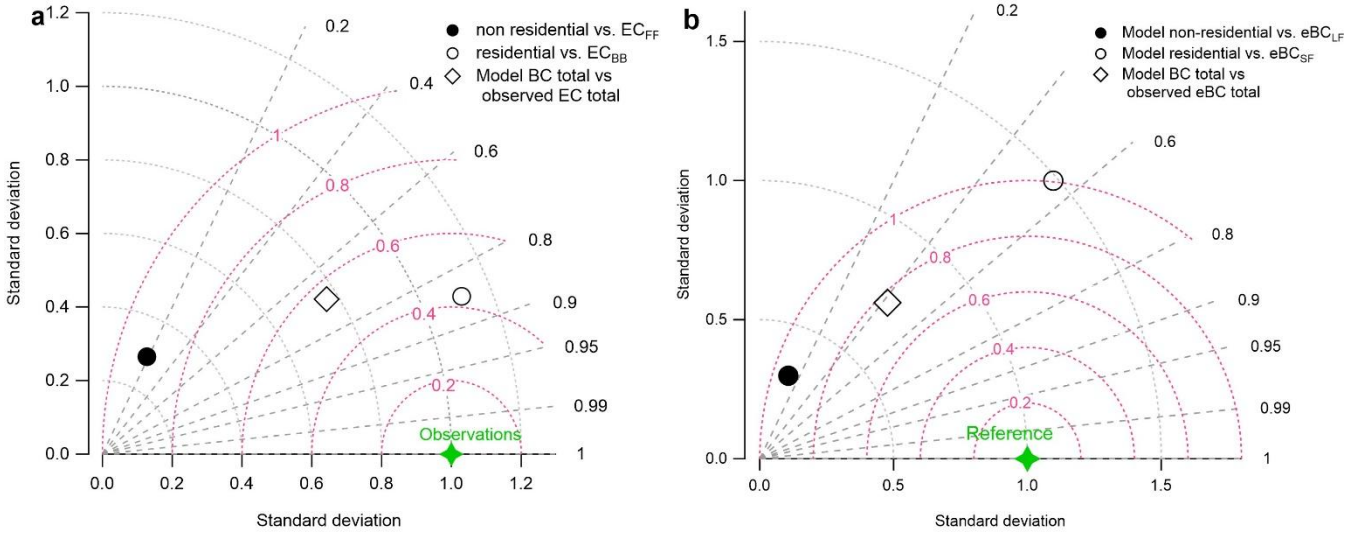

Figure 12: Taylor diagrams comparing modelled BC sources with EC and eBC tracers and NNMF factors. Each panel shows three model–observation pairs (symbols per legend). The green diamond marks the reference (observations) at unit standard deviation. Grey dashed semicircles are isolines marking radial distance from the origin of standard deviation modelled/ standard deviation observed. Values under one represent under dispersion of the model and over one represent over dispersion of the model. Grey

https://doi.org/10.5194/egusphere-2026-1708
Preprint. Discussion started: 10 August 2026

radial spokes show the angle from the x-axis, measuring linear correlation as Pearson's R^2. Magenta dashed arcs are contours of normalised centred root mean square deviation (RMSD), i.e., the Euclidean distance to the green diamond. Smaller values indicate better overall agreement. Better performance over all three metrics is thus indicated by proximity to the reference point. a) Filled circle: Non-residential model (all model sources except residential) vs EC_{FF} (fossil-fuel EC). Open circle: Residential-only model vs EC_{BB} (biomass-burning EC). Open diamond: Model BC total vs observed EC. b) Filled circle: Non-residential model vs NNMF eBC_{SF}, Open circle: residential-only model vs NNMF eBC_{LF}. Open diamond: Model BC total vs observed eBC.

4 Conclusions

We have provided continuous, year-round observations and source apportionment (SA) of carbonaceous aerosol in Belgrade (Ada Marina), addressing a major observational gap in the Western Balkans where accessible long-term measurements remain scarce. Ada Marina exhibits low pollution levels for eBC in a Southeastern European, urban, setting and somewhat elevated PM_{10} concentrations: values remain well below current national limit values aligned with the EU Ambient Air Quality Directive (AAQD), but exceed WHO guideline levels and the forthcoming EU AAQD annual PM_{10} limit scheduled for implementation in 2030.

All three SA approaches applied here (offline organic tracers, the aethalometer model, and a novel NNMF framework) consistently identify residential wood combustion (RWC) as a major wintertime source of eBC and EC while offline tracers show it is also a dominant source of OC. The seasonal contrast is pronounced. Biomass-burning contributions account for nearly half of EC during winter but only a small fraction in summer. Similar seasonal patterns are reproduced by the aethalometer model and NNMF. Strong wintertime correlations between secondary organic carbon (SOC) and biomass-burning tracers further indicate that RWC emissions contribute not only to primary carbonaceous aerosol but also to secondary organic aerosol formation. Additional evidence arises from enhanced wintertime brown-carbon absorption, which NNMF attributes entirely to solid-fuel combustion.

Transport modelling using FLEXPART supports these findings. Residential-emission tracers in the model correlate strongly with both EC_{BB} and the NNMF-derived solid-fuel eBC component. Our analysis indicates that Belgrade's carbonaceous aerosol burden reflects a combination of national emissions and regional transport, with episodic enhancements originating from the Pannonian Basin and surrounding regions. The good agreement between modelled residential emissions and observations suggests that regional-scale emission changes could be meaningfully evaluated using the diagnostics applied here.

Given the consistent identification of RWC as a dominant wintertime contributor across this and other studies in South-Eastern Europe, reductions in emissions from this sector could substantially influence regional PM burdens. However, the effectiveness of such mitigation is likely constrained by both transboundary transport and socioeconomic factors related to residential heating practices. Studies such as the present work therefore provide an important scientific basis for understanding source contributions and evaluating potential emission-change scenarios. Methodologically, the results highlight the value of combining complementary SA approaches. In particular, NNMF proved effective in resolving spectral deviations without requiring a priori Ångström exponents, while reproducing the results of established tracer-based methods. Although a three-

https://doi.org/10.5194/egusphere-2026-1708
Preprint. Discussion started: 10 August 2026

factor NNMF solution was not supported for this dataset, the NNMF approach remains flexible and readily transferable to other locations or multi-site analyses.

Code and data availability

The code used for the source apportionment of online absorption data is available at Zenodo: 10.5281/zenodo.19221204 (Platt et al., 2026). Atmospheric data used in this study are available under the WeBaSOOP framework at EBAS: https://ebas-data.nilu.no/Pages/DataSetList.aspx?key=F4D521229C2A40F9A3F9E158848FB229.

Supplement link

Disclaimer

Copernicus Publications remains neutral with regard to jurisdictional claims made in the text, published maps, institutional affiliations, or any other geographical representation in this paper. While Copernicus Publications makes every effort to include appropriate place names, the final responsibility lies with the authors. Views expressed in the text are those of the authors and do not necessarily reflect the views of the publisher

Author contributions

S.M.P. conceived the study, developed the methodology, performed the analysis, and wrote the manuscript. K.E.Y. contributed to the manuscript and developed the tracer-based source apportionment approach. M.J. and Ž.Ć. contributed to the site description. B.P. performed the tracer laboratory analyses, and H.G. conducted the EC/OC analyses. M.D. and Ž.Ć. operated the aethalometer measurements. P.S. performed the mapping analysis. S.E. and N.E. conducted the FLEXPART modelling and analysis. All authors contributed to the interpretation of the results and to the final version of the manuscript.

Competing interests

The authors declare no competing interests.

https://doi.org/10.5194/egusphere-2026-1708
Preprint. Discussion started: 10 August 2026

Acknowledgements

This research was funded by: The European Union's Horizon Europe Research and Innovation Program under GA 101060170 (WeBaSOOP project), the European Union's Horizon Europe research and innovation program (101081395; EYE-CLIMA) and the Ministry of Science, Technological Development and Innovation of the Republic of Serbia under GA 451-03-136/2025-03/200017. FLEXPART model simulations are cross-atmospheric research infrastructure services provided by ATMO-ACCESS (EU grant agreement No 101008004). Nikolaos Evangeliou was funded by the same EU grant. The computations were performed on resources provided by Sigma2 - the National Infrastructure for High Performance Computing and Data Storage in Norway. AI tools were used for language editing and clarity improvement.

References

ACTRIS: ACTRIS Standard Operating Procedure for AE33 Aethalometer Measurements, https://www.actris-ecac.eu/pluginAppObj/pluginAppObj_225_189/2021-09-14_ACTRIS_AE33_v1.pdf, last access: 19.03.2026, ACTRIS, 2021.

Andreae, M. O. and Gelencsér, A.: Black carbon or brown carbon? The nature of light-absorbing carbonaceous aerosols, Atmos. Chem. Phys., 6, 3131-3148, 10.5194/acp-6-3131-2006, 2006.

Basnet, S., Hartikainen, A., Virkkula, A., Yli-Pirilä, P., Kortelainen, M., Suhonen, H., Kilpeläinen, L., Ihalainen, M., Väätäinen, S., Louhisalmi, J., Somero, M., Tissari, J., Jakobi, G., Zimmermann, R., Kilpeläinen, A., and Sippula, O.: Contribution of brown carbon to light absorption in emissions of European residential biomass combustion appliances, Atmos. Chem. Phys., 24, 3197-3215, 10.5194/acp-24-3197-2024, 2024.

Bauer, H., Kasper-Giebl, A., Löflund, M., Giebl, H., Hitzenberger, R., Zibuschka, F., and Puxbaum, H.: The contribution of bacteria and fungal spores to the organic carbon content of cloud water, precipitation and aerosols, Atmospheric Research, 64, 109-119, https://doi.org/10.1016/S0169-8095(02)00084-4, 2002.

Belis, C. A., Karagulian, F., Larsen, B. R., and Hopke, P. K.: Critical review and meta-analysis of ambient particulate matter source apportionment using receptor models in Europe, Atmospheric Environment, 69, 94-108, https://doi.org/10.1016/j.atmosenv.2012.11.009, 2013.

Belis, C. A., Pisoni, E., Degraeuwe, B., Peduzzi, E., Thunis, P., Monforti-Ferrario, F., and Guizzardi, D.: Urban pollution in the Danube and Western Balkans regions: The impact of major PM2.5 sources, Environment International, 133, 105158, https://doi.org/10.1016/j.envint.2019.105158, 2019.

Bond, T. C., Doherty, S. J., Fahey, D. W., Forster, P. M., Berntsen, T., DeAngelo, B. J., Flanner, M. G., Ghan, S., Kärcher, B., Koch, D., Kinne, S., Kondo, Y., Quinn, P. K., Sarofim, M. C., Schultz, M. G., Schulz, M., Venkataraman, C., Zhang, H., Zhang, S., Bellouin, N., Guttikunda, S. K., Hopke, P. K., Jacobson, M. Z., Kaiser, J. W., Klimont, Z., Lohmann, U., Schwarz, J. P., Shindell, D., Storelvmo, T., Warren, S. G., and Zender, C. S.: Bounding the role of black carbon in the climate system: A scientific assessment, Journal of Geophysical Research: Atmospheres, 118, 5380-5552, https://doi.org/10.1002/jgrd.50171, 2013.

Caseiro, A., Bauer, H., Schmidl, C., Pio, C. A., and Puxbaum, H.: Wood burning impact on PM10 in three Austrian regions, Atmospheric Environment, 43, 2186-2195, https://doi.org/10.1016/j.atmosenv.2009.01.012, 2009.

Cassiani, M., Stohl, A., and Brioude, J.: Lagrangian Stochastic Modelling of Dispersion in the Convective Boundary Layer with Skewed Turbulence Conditions and a Vertical Density Gradient: Formulation and Implementation in the FLEXPART Model, Boundary-Layer Meteorology, 154, 367-390, 10.1007/s10546-014-9976-5, 2015.

Cavalli, F., Viana, M., Yttri, K. E., Genberg, J., and Putaud, J. P.: Toward a standardised thermal-optical protocol for measuring atmospheric organic and elemental carbon: the EUSAAR protocol, Atmos. Meas. Tech., 3, 79-89, 10.5194/amt-3-79-2010, 2010.

Chen, G., Canonaco, F., Tobler, A., Aas, W., Alastuey, A., Allan, J., Atabakhsh, S., Aurela, M., Baltensperger, U., Bougiatioti, A., De Brito, J. F., Ceburnis, D., Chazeau, B., Chebaicheb, H., Daellenbach, K. R., Ehn, M., El Haddad, I., Eleftheriadis, K., Favez, O., Flentje, H., Font, A., Fossum, K., Freney, E., Gini, M., Green, D. C., Heikkinen, L., Herrmann, H., Kalogridis, A.-C., Keernik, H., Lhotka, R., Lin, C., Lunder, C., Maasikmets, M., Manousakas, M. I., Marchand, N., Marin, C., Marmureanu, L., Mihalopoulos, N., Močnik, G., Nęcki, J., O'Dowd, C., Ovadnevaite, J., Peter, T., Petit, J.-E., Pikridas, M., Matthew Platt,

https://doi.org/10.5194/egusphere-2026-1708
Preprint. Discussion started: 10 August 2026

S., Pokorná, P., Poulain, L., Priestman, M., Riffault, V., Rinaldi, M., Różański, K., Schwarz, J., Sciare, J., Simon, L., Skiba, A., Slowik, J. G., Sosedova, Y., Stavroulas, I., Styszko, K., Teinemaa, E., Timonen, H., Tremper, A., Vasilescu, J., Via, M., Vodička, P., Wiedensohler, A., Zografou, O., Cruz Minguillón, M., and Prévôt, A. S. H.: European aerosol phenomenology − 8: Harmonised source apportionment of organic aerosol using 22 Year-long ACSM/AMS datasets, Environment International, 166, 107325, https://doi.org/10.1016/j.envint.2022.107325, 2022.

Ćirović, Ž., Stojanović, D., Davidović, M., Živković, M., Jovanović, M., Onjia, A., and Jovašević Stojanović, M.: Preliminary analysis of diurnal and seasonal variation of submicron ambient particle size distribution in Belgrade urban area, WeBIOPATR 2023: 9th WeBIOPATR Workshop & Conference: Particulate Matter: Research and Management: Abstracts of Keynote Invited Lectures and Contributed Papers, 106-111,

Diapouli, E., Kalogridis, A.-C., Markantonaki, C., Vratolis, S., Fetfatzis, P., Colombi, C., and Eleftheriadis, K.: Annual Variability of Black Carbon Concentrations Originating from Biomass and Fossil Fuel Combustion for the Suburban Aerosol in Athens, Greece, 10.3390/atmos8120234, 2017.

Drinovec, L., Močnik, G., Zotter, P., Prévôt, A. S. H., Ruckstuhl, C., Coz, E., Rupakheti, M., Sciare, J., Müller, T., Wiedensohler, A., and Hansen, A. D. A.: The "dual-spot" Aethalometer: an improved measurement of aerosol black carbon with real-time loading compensation, Atmos. Meas. Tech., 8, 1965-1979, 10.5194/amt-8-1965-2015, 2015.

El Haddad, I., Marchand, N., Wortham, H., Piot, C., Besombes, J. L., Cozic, J., Chauvel, C., Armengaud, A., Robin, D., and Jaffrezo, J. L.: Primary sources of PM_{2.5} organic aerosol in an industrial Mediterranean city, Marseille, Atmos. Chem. Phys., 11, 2039-2058, 10.5194/acp-11-2039-2011, 2011.

European Parliament and Council: Directive (EU) 2024/2881 of the European Parliament and of the Council of 23 October 2024 on ambient air quality and cleaner air for Europe (recast), 2024.

Favez, O., El Haddad, I., Piot, C., Boréave, A., Abidi, E., Marchand, N., Jaffrezo, J. L., Besombes, J. L., Personnaz, M. B., Sciare, J., Wortham, H., George, C., and D'Anna, B.: Inter-comparison of source apportionment models for the estimation of wood burning aerosols during wintertime in an Alpine city (Grenoble, France), Atmos. Chem. Phys., 10, 5295-5314, 10.5194/acp-10-5295-2010, 2010.

Forrister, H., Liu, J., Scheuer, E., Dibb, J., Ziemba, L., Thornhill, K. L., Anderson, B., Diskin, G., Perring, A. E., Schwarz, J. P., Campuzano-Jost, P., Day, D. A., Palm, B. B., Jimenez, J. L., Nenes, A., and Weber, R. J.: Evolution of brown carbon in wildfire plumes, Geophysical Research Letters, 42, 4623-4630, https://doi.org/10.1002/2015GL063897, 2015.

Forster, C., Stohl, A., and Seibert, P.: Parameterization of Convective Transport in a Lagrangian Particle Dispersion Model and Its Evaluation, Journal of Applied Meteorology and Climatology, 46, 403-422, https://doi.org/10.1175/JAM2470.1, 2007.

Gan, W. Q., Koehoorn, M., Davies, H. W., Demers, P. A., Tamburic, L., and Brauer, M.: Long-term exposure to traffic-related air pollution and the risk of coronary heart disease hospitalization and mortality, Environmental health perspectives, 119, 501-507, 10.1289/ehp.1002511, 2011.

Gilardoni, S., Vignati, E., Cavalli, F., Putaud, J. P., Larsen, B. R., Karl, M., Stenström, K., Genberg, J., Henne, S., and Dentener, F.: Better constraints on sources of carbonaceous aerosols using a combined ¹⁴C – macro tracer analysis in a European rural background site, Atmos. Chem. Phys., 11, 5685-5700, 10.5194/acp-11-5685-2011, 2011.

Gilardoni, S., Massoli, P., Paglione, M., Giulianelli, L., Carbone, C., Rinaldi, M., Decesari, S., Sandrini, S., Costabile, F., Gobbi, G. P., Pietrogrande, M. C., Visentin, M., Scotto, F., Fuzzi, S., and Facchini, M. C.: Direct observation of aqueous secondary organic aerosol from biomass-burning emissions, Proceedings of the National Academy of Sciences, 113, 10013-10018, 10.1073/pnas.1602212113, 2016.

Glojek, K., Dinh Ngoc Thuy, V., Weber, S., Uzu, G., Manousakas, M., Elazzouzi, R., Džepina, K., Darfeuil, S., Ginot, P., Jaffrezo, J. L., Žabkar, R., Turšič, J., Podkoritnik, A., and Močnik, G.: Annual variation of source contributions to PM10 and oxidative potential in a mountainous area with traffic, biomass burning, cement-plant and biogenic influences, Environment International, 189, 108787, https://doi.org/10.1016/j.envint.2024.108787, 2024.

Grythe, H., Kristiansen, N. I., Groot Zwaaftink, C. D., Eckhardt, S., Ström, J., Tunved, P., Krejci, R., and Stohl, A.: A new aerosol wet removal scheme for the Lagrangian particle model FLEXPART v10, Geosci. Model Dev., 10, 1447-1466, 10.5194/gmd-10-1447-2017, 2017.

Hadley, O. L. and Kirchstetter, T. W.: Black-carbon reduction of snow albedo, Nature Climate Change, 2, 437-440, 10.1038/nclimate1433, 2012.

Heald, C. L. and Spracklen, D. V.: Atmospheric budget of primary biological aerosol particles from fungal spores, Geophysical Research Letters, 36, https://doi.org/10.1029/2009GL037493, 2009.

https://doi.org/10.5194/egusphere-2026-1708
Preprint. Discussion started: 10 August 2026

Helin, A., Virkkula, A., Backman, J., Pirjola, L., Sippula, O., Aakko-Saksa, P., Väätäinen, S., Mylläri, F., Järvinen, A., Bloss, M., Aurela, M., Jakobi, G., Karjalainen, P., Zimmermann, R., Jokiniemi, J., Saarikoski, S., Tissari, J., Rönkkö, T., Niemi, J. V., and Timonen, H.: Variation of Absorption Ångström Exponent in Aerosols From Different Emission Sources, Journal of Geophysical Research: Atmospheres, 126, e2020JD034094, https://doi.org/10.1029/2020JD034094, 2021.

Hersbach, H., Bell, B., Berrisford, P., Hirahara, S., Horányi, A., Muñoz-Sabater, J., Nicolas, J., Peubey, C., Radu, R., Schepers, D., Simmons, A., Soci, C., Abdalla, S., Abellan, X., Balsamo, G., Bechtold, P., Biavati, G., Bidlot, J., Bonavita, M., De Chiara, G., Dahlgren, P., Dee, D., Diamantakis, M., Dragani, R., Flemming, J., Forbes, R., Fuentes, M., Geer, A., Haimberger, L., Healy, S., Hogan, R. J., Hólm, E., Janisková, M., Keeley, S., Laloyaux, P., Lopez, P., Lupu, C., Radnoti, G., de Rosnay, P., Rozum, I., Vamborg, F., Villaume, S., and Thépaut, J.-N.: The ERA5 global reanalysis, Quarterly Journal of the Royal Meteorological Society, 146, 1999-2049, https://doi.org/10.1002/qj.3803, 2020.

Huremović, J., Žero, S., Bubalo, E., Dacić, M., Čeliković, A., Musić, I., Bašić, M., Huseinbašić, N., Džepina, K., Cepić, M., Muratović, N., Pašalić, A., Salihagić, S., Krvavac, Z., Zelić-Hadžiomerović, J., and Gojak-Salimović, S.: Analysis of PM10, Pb, Cd, and Ni atmospheric concentrations during domestic heating season in Sarajevo, Bosnia and Herzegovina, from 2010 to 2019, Air Quality, Atmosphere & Health, 13, 965-976, 10.1007/s11869-020-00852-4, 2020.

IPCC: Climate change 2021: the physical science basis, Cambridge University Press, Cambridge, United Kingdom and New York, NY, USA, 2391, 10.1017/9781009157896, 2021.

Jacobson, M. Z.: Control of fossil-fuel particulate black carbon and organic matter, possibly the most effective method of slowing global warming, Journal of Geophysical Research: Atmospheres, 107, ACH 16-11-ACH 16-22, https://doi.org/10.1029/2001JD001376, 2002.

Jiang, F., Saathoff, H., Ezenobi, U., Song, J., Zhang, H., Gao, L., and Leisner, T.: Measurement report: Brown carbon aerosol in rural Germany – sources, chemistry, and diurnal variations, Atmos. Chem. Phys., 25, 1917-1930, 10.5194/acp-25-1917-2025, 2025.

Jovanović, M. V., Savić, J., Kovačević, R., Tasić, V., Todorović, Ž., Stevanović, S., Manojlović, D., and Jovašević-Stojanović, M.: Comparison of fine particulate matter level, chemical content and oxidative potential derived from two dissimilar urban environments, Science of The Total Environment, 708, 135209, https://doi.org/10.1016/j.scitotenv.2019.135209, 2020.

Kaiser, J. W., Heil, A., Andreae, M. O., Benedetti, A., Chubarova, N., Jones, L., Morcrette, J. J., Razinger, M., Schultz, M. G., Suttie, M., and van der Werf, G. R.: Biomass burning emissions estimated with a global fire assimilation system based on observed fire radiative power, Biogeosciences, 9, 527-554, 10.5194/bg-9-527-2012, 2012.

Kalbermatter, D. M., Močnik, G., Drinovec, L., Visser, B., Röhrbein, J., Oscity, M., Weingartner, E., Hyvärinen, A. P., and Vasilatou, K.: Comparing black-carbon- and aerosol-absorption-measuring instruments – a new system using lab-generated soot coated with controlled amounts of secondary organic matter, Atmos. Meas. Tech., 15, 561-572, 10.5194/amt-15-561-2022, 2022.

Kirchstetter, T. W., Novakov, T., and Hobbs, P. V.: Evidence that the spectral dependence of light absorption by aerosols is affected by organic carbon, Journal of Geophysical Research: Atmospheres, 109, https://doi.org/10.1029/2004JD004999, 2004.

Klimont, Z., Heyes, C., Rafaj, P., Hoglund-Isaksson, L., Purohit, P., Kaltenegger, K., Gomez-Sanabria, A., Kim, Y., Winiwarter, W., Warnecke, L., Schoepp, W., Lindl, F., Kiesewetter, G., Sander, R., Nguyen, B., Zhang, S., Brocza, F., & Wagner, F. : Global gridded anthropogenic emissions of air pollutants and methane for the period 1990-2050 [dataset], https://doi.org/10.5281/zenodo.14259955, 2024.

Kumar, N. K., Corbin, J. C., Bruns, E. A., Massabó, D., Slowik, J. G., Drinovec, L., Močnik, G., Prati, P., Vlachou, A., Baltensperger, U., Gysel, M., El-Haddad, I., and Prévôt, A. S. H.: Production of particulate brown carbon during atmospheric aging of residential wood-burning emissions, Atmos. Chem. Phys., 18, 17843-17861, 10.5194/acp-18-17843-2018, 2018.

Laskin, A., Laskin, J., and Nizkorodov, S. A.: Chemistry of Atmospheric Brown Carbon, Chemical Reviews, 115, 4335-4382, 10.1021/cr5006167, 2015.

Lee, D. D. and Seung, H. S.: Learning the parts of objects by non-negative matrix factorization, Nature, 401, 788-791, 10.1038/44565, 1999.

Lee, L. A., Reddington, C. L., and Carslaw, K. S.: On the relationship between aerosol model uncertainty and radiative forcing uncertainty, Proceedings of the National Academy of Sciences, 113, 5820-5827, 10.1073/pnas.1507050113, 2016.

Levin, E. J. T., McMeeking, G. R., Carrico, C. M., Mack, L. E., Kreidenweis, S. M., Wold, C. E., Moosmüller, H., Arnott, W. P., Hao, W. M., Collett Jr, J. L., and Malm, W. C.: Biomass burning smoke aerosol properties measured during Fire Laboratory

https://doi.org/10.5194/egusphere-2026-1708
Preprint. Discussion started: 10 August 2026

at Missoula Experiments (FLAME), Journal of Geophysical Research: Atmospheres, 115, https://doi.org/10.1029/2009JD013601, 2010.
Liang, C.-S., Yue, D., Wu, H., Shi, J.-S., and He, K.-B.: Source apportionment of atmospheric particle number concentrations with wide size range by nonnegative matrix factorization (NMF), Environmental Pollution, 289, 117846, https://doi.org/10.1016/j.envpol.2021.117846, 2021.
Liu, H., Pan, X., Lei, S., Zhang, Y., Du, A., Yao, W., Tang, G., Wang, T., Xin, J., Li, J., Sun, Y., Cao, J., and Wang, Z.: Vertical distribution of black carbon and its mixing state in the urban boundary layer in summer, Atmos. Chem. Phys., 23, 7225-7239, 10.5194/acp-23-7225-2023, 2023.
Liu, S., Aiken, A. C., Gorkowski, K., Dubey, M. K., Cappa, C. D., Williams, L. R., Herndon, S. C., Massoli, P., Fortner, E. C., Chhabra, P. S., Brooks, W. A., Onasch, T. B., Jayne, J. T., Worsnop, D. R., China, S., Sharma, N., Mazzoleni, C., Xu, L., Ng, N. L., Liu, D., Allan, J. D., Lee, J. D., Fleming, Z. L., Mohr, C., Zotter, P., Szidat, S., and Prévôt, A. S. H.: Enhanced light absorption by mixed source black and brown carbon particles in UK winter, Nature Communications, 6, 8435, 10.1038/ncomms9435, 2015.
Marsavin, A., van Gageldonk, R., Bernays, N., May, N. W., Jaffe, D. A., and Fry, J. L.: Optical properties of biomass burning aerosol during the 2021 Oregon fire season: comparison between wild and prescribed fires, Environmental Science: Atmospheres, 3, 608-626, 10.1039/D2EA00118G, 2023.
Masić, A. D. M., E.; Duraković, M.; Prćanović, H.: New Insight into Black Carbon Analysis of Strong Air Pollution Episodes, 35th DAAAM International Symposium on Intelligent Manufacturing and Automation, Vienna, 10.2507/35th.daaam.proceedings.013,
Massabò, D., Caponi, L., Bernardoni, V., Bove, M. C., Brotto, P., Calzolai, G., Cassola, F., Chiari, M., Fedi, M. E., Fermo, P., Giannoni, M., Lucarelli, F., Nava, S., Piazzalunga, A., Valli, G., Vecchi, R., and Prati, P.: Multi-wavelength optical determination of black and brown carbon in atmospheric aerosols, Atmospheric Environment, 108, 1-12, https://doi.org/10.1016/j.atmosenv.2015.02.058, 2015.
World Bank: Western Balkans Green Resilient and Digital Development (GRDD) Regional Program blogs.worldbank.org/en/transport/road-emissions-in-the-western-balkans-, last access: 05.03.2026.
Paisi, N., Kushta, J., Pozzer, A., Violaris, A., and Lelieveld, J.: Health effects of carbonaceous PM2.5 compounds from residential fuel combustion and road transport in Europe, Sci Rep, 14, 1530, 10.1038/s41598-024-51916-9, 2024.
Pajic, N., Jurišević, N., and Despotovic, M.: Adoption of Electric Vehicles in the Republic of Serbia, Transportation in Developing Economies, 10, 33, 10.1007/s40890-024-00220-2, 2024.
Petrović, B., Petrović, B., Alastuey, A., Yttri, K. E., Pandolfi, M., Platt, S. M., Bartonova, A., and Stojanović, M. J.: Source apportionment of PM10 mass concentration in an urban background site in Belgrade, Serbia in Prep.
Petzold, A., Ogren, J. A., Fiebig, M., Laj, P., Li, S. M., Baltensperger, U., Holzer-Popp, T., Kinne, S., Pappalardo, G., Sugimoto, N., Wehrli, C., Wiedensohler, A., and Zhang, X. Y.: Recommendations for reporting "black carbon" measurements, Atmos. Chem. Phys., 13, 8365-8379, 10.5194/acp-13-8365-2013, 2013.
Pisso, I., Sollum, E., Grythe, H., Kristiansen, N. I., Cassiani, M., Eckhardt, S., Arnold, D., Morton, D., Thompson, R. L., Groot Zwaaftink, C. D., Evangeliou, N., Sodemann, H., Haimberger, L., Henne, S., Brunner, D., Burkhart, J. F., Fouilloux, A., Brioude, J., Philipp, A., Seibert, P., and Stohl, A.: The Lagrangian particle dispersion model FLEXPART version 10.4, Geosci. Model Dev., 12, 4955-4997, 10.5194/gmd-12-4955-2019, 2019.
Platt, S. M.: Source apportionment of multi-wavelength aerosol absorption using NNMF and aethalometer-based methods (Igor Pro code), https://doi.org/10.5281/zenodo.19221205, 2026.
Platt, S. M., El Haddad, I., Pieber, S. M., Zardini, A. A., Suarez-Bertoa, R., Clairotte, M., Daellenbach, K. R., Huang, R. J., Slowik, J. G., Hellebust, S., Temime-Roussel, B., Marchand, N., de Gouw, J., Jimenez, J. L., Hayes, P. L., Robinson, A. L., Baltensperger, U., Astorga, C., and Prévôt, A. S. H.: Gasoline cars produce more carbonaceous particulate matter than modern filter-equipped diesel cars, Scientific Reports, 7, 4926, 10.1038/s41598-017-03714-9, 2017.
Popovicheva, O., Chichaeva, M., Kovach, R., Zhdanova, E., and Kasimov, N.: Seasonal, Weekly, and Diurnal Black Carbon in Moscow Megacity Background under Impact of Urban and Regional Sources, 10.3390/atmos13040563, 2022.
Putaud, J.-P., Cavalli, F., Yttri, K. E., Chow, J. C., Watson, J. G., Sinha, B., Venkataraman, C., Ikemori, F., Jaffrezo, J.-L., Uzu, G., Moreno, I., Krejci, R., Laj, P., Gupta, T., Hu, M., Kim, S.-W., Mayol-Bracero, O., Quinn, P., Aas, W., Alastuey, A., Andrade, M., Angelucci, M., Anurag, G., Beukes, J. P., Bhardwaj, A., Chatterjee, A., Chaudhary, P., Chhangani, A. K., Conil, S., Degorska, A., Devaliya, S., Dhandapani, A., Duhan, S. S., Chandra Dumka, U., Habib, G., Hamzavi, Z., Haswani, D.,

https://doi.org/10.5194/egusphere-2026-1708
Preprint. Discussion started: 10 August 2026

Herrmann, H., Holubova, A., Hueglin, C., Imran, M., Jehangir, A., Kapoor, T. S., Karanasiou, A., Khaiwal, R., Kim, J., Kolesa, T., Kozakiewicz, J., Kranjc, I., Laura, J. S., Lian, Y., Liu, J., Manwani, P., Mardoñez-Balderrama, V., Marticorena, B., Matsuki, A., Mor, S., Mukherjee, S., Murthy, S., Muthalagu, A., Najar, T. A., Kumar, R. N., Pandithurai, G., Perez, N., Phairuang, W., Phuleria, H. C., Poulain, L., Prasad, L., Pullokaran, D., Qadri, A. M., Qureshi, A., Ramírez, O., Roy, S., Rüdiger, J., Saikia, B. K., Saikia, P., Sauvage, S., Savvides, C., Sharma, R., Singh, T., Singh, G. K., Spoor, R., Srivastava, A. K., Raman, R. S., Van Zyl, P. G., Vecchiocattivi, M., Voiron, C., Xin, J., and Yadav, K.: A worldwide aerosol phenomenology: Elemental and organic carbon in PM2.5 and PM10, Atmospheric Environment, 358, 121338, https://doi.org/10.1016/j.atmosenv.2025.121338, 2025.

Paatero, P. and Tapper, U.: Positive matrix factorization: A non-negative factor model with optimal utilization of error estimates of data values, Environmetrics, 5, 111-126, https://doi.org/10.1002/env.3170050203, 1994.

Rathbone, C. J., Bousiotis, D., Rose, O. G., and Pope, F. D.: Using low-cost sensors to assess common air pollution sources across multiple residences, Scientific Reports, 15, 1803, 10.1038/s41598-025-85985-1, 2025.

Reff, A., I., E. S., and and Bhave, P. V.: Receptor Modeling of Ambient Particulate Matter Data Using Positive Matrix Factorization: Review of Existing Methods, Journal of the Air & Waste Management Association, 57, 146-154, 10.1080/10473289.2007.10465319, 2007.

Republic of Serbia: Air Quality Programme of the Republic of Serbia for the Period 2022–2030 with an Action Plan, 2023.

Robinson, A. L., Donahue, N. M., Shrivastava, M. K., Weitkamp, E. A., Sage, A. M., Grieshop, A. P., Lane, T. E., Pierce, J. R., and Pandis, S. N.: Rethinking Organic Aerosols: Semivolatile Emissions and Photochemical Aging, Science, 315, 1259-1262, 10.1126/science.1133061, 2007.

Saleh, R., Robinson, E. S., Tkacik, D. S., Ahern, A. T., Liu, S., Aiken, A. C., Sullivan, R. C., Presto, A. A., Dubey, M. K., Yokelson, R. J., Donahue, N. M., and Robinson, A. L.: Brownness of organics in aerosols from biomass burning linked to their black carbon content, Nature Geoscience, 7, 647-650, 10.1038/ngeo2220, 2014.

Sandradewi, J., Prévôt, A. S. H., Weingartner, E., Schmidhauser, R., Gysel, M., and Baltensperger, U.: A study of wood burning and traffic aerosols in an Alpine valley using a multi-wavelength Aethalometer, Atmospheric Environment, 42, 101-112, https://doi.org/10.1016/j.atmosenv.2007.09.034, 2008a.

Sandradewi, J., Prévôt, A. S. H., Szidat, S., Perron, N., Alfarra, M. R., Lanz, V. A., Weingartner, E., and Baltensperger, U.: Using Aerosol Light Absorption Measurements for the Quantitative Determination of Wood Burning and Traffic Emission Contributions to Particulate Matter, Environmental Science & Technology, 42, 3316-3323, 10.1021/es702253m, 2008b.

Savadkoohi, M., Gherras, M., Favez, O., Petit, J.-E., Rovira, J., Chen, G. I., Via, M., Platt, S., Aurela, M., Chazeau, B., de Brito, J. F., Riffault, V., Eleftheriadis, K., Flentje, H., Gysel-Beer, M., Hueglin, C., Rigler, M., Gregorič, A., Ivančič, M., Keernik, H., Maasikmets, M., Liakakou, E., Stavroulas, I., Luoma, K., Marchand, N., Mihalopoulos, N., Petäjä, T., Prevot, A. S. H., Daellenbach, K. R., Vodička, P., Timonen, H., Tobler, A., Vasilescu, J., Dandocsi, A., Mbengue, S., Vratolis, S., Zografou, O., Chauvigné, A., Hopke, P. K., Querol, X., Alastuey, A., and Pandolfi, M.: Addressing the advantages and limitations of using Aethalometer data to determine the optimal absorption Ångström exponents (AAEs) values for eBC source apportionment, Atmospheric Environment, 349, 121121, https://doi.org/10.1016/j.atmosenv.2025.121121, 2025.

Savadkoohi, M., Pandolfi, M., Reche, C., Niemi, J. V., Mooibroek, D., Titos, G., Green, D. C., Tremper, A. H., Hueglin, C., Liakakou, E., Mihalopoulos, N., Stavroulas, I., Artiñano, B., Coz, E., Alados-Arboledas, L., Beddows, D., Riffault, V., De Brito, J. F., Bastian, S., Baudic, A., Colombi, C., Costabile, F., Chazeau, B., Marchand, N., Gómez-Amo, J. L., Estellés, V., Matos, V., van der Gaag, E., Gille, G., Luoma, K., Manninen, H. E., Norman, M., Silvergren, S., Petit, J.-E., Putaud, J.-P., Rattigan, O. V., Timonen, H., Tuch, T., Merkel, M., Weinhold, K., Vratolis, S., Vasilescu, J., Favez, O., Harrison, R. M., Laj, P., Wiedensohler, A., Hopke, P. K., Petäjä, T., Alastuey, A., and Querol, X.: The variability of mass concentrations and source apportionment analysis of equivalent black carbon across urban Europe, Environment International, 178, 108081, https://doi.org/10.1016/j.envint.2023.108081, 2023.

SEPA: Annual Report on the State of Air Quality in the Republic of Serbia: 2023, Ministry of Environmental Protection, Republic of Serbia, Belgrade, Serbia, 2024.

Serbian Environmental Protection Agency – Official Website: https://sepa.gov.rs/?id&akcija=showHome, last access: 13 June 2025.

Skiba, A., Styszko, K., Tobler, A., Casotto, R., Gorczyca, Z., Furman, P., Samek, L., Wideł, D., Zimnoch, M., Kasper-Giebl, A., Slowik, J. G., Daellenbach, K. R., Prevot, A. S. H., and Różański, K.: Source attribution of carbonaceous fraction of

https://doi.org/10.5194/egusphere-2026-1708
Preprint. Discussion started: 10 August 2026

particulate matter in the urban atmosphere based on chemical and carbon isotope composition, Scientific Reports, 14, 7234, 10.1038/s41598-024-57829-x, 2024.
Sopčić, S., Godec, R., Jakovljević, I., and Bešlić, I.: The Influence of Biomass Burning on the Organic Content of Urban Aerosols, 10.3390/biomass5010001, 2025.
Stohl, A., Forster, C., Frank, A., Seibert, P., and Wotawa, G.: Technical note: The Lagrangian particle dispersion model FLEXPART version 6.2, Atmos. Chem. Phys., 5, 2461-2474, 10.5194/acp-5-2461-2005, 2005.
Szopa, S., Naik, V., Adhikary, B., Artaxo, P., Berntsen, T., Collins, W. D., Fuzzi, S., Gallardo, L., Kiendler-Scharr, A., Klimont, Z., Liao, H., Unger, N., and Zanis, P.: Short-Lived Climate Forcers (Chapter 6), Cambridge University Press, Cambridge, United Kingdom and New York, NY, USA, 10.1017/9781009157896.008, 2021.
Targa, J., Ripoll, A., Banyuls, L., González Ortiz, A., and Soares, J.: Status Report of Air Quality in Europe for Year 2022, 2022.
Theodosi, C., Grivas, G., Zarmpas, P., Chaloulakou, A., and Mihalopoulos, N.: Mass and chemical composition of size-segregated aerosols (PM₁, PM_{2.5}, PM₁₀) over Athens, Greece: local versus regional sources, Atmos. Chem. Phys., 11, 11895-11911, 10.5194/acp-11-11895-2011, 2011.
Tobler, A. K., Skiba, A., Canonaco, F., Močnik, G., Rai, P., Chen, G., Bartyzel, J., Zimnoch, M., Styszko, K., Nęcki, J., Furger, M., Różański, K., Baltensperger, U., Slowik, J. G., and Prevot, A. S. H.: Characterization of non-refractory (NR) PM1 and source apportionment of organic aerosol in Kraków, Poland, Atmos. Chem. Phys., 21, 14893-14906, 10.5194/acp-21-14893-2021, 2021.
Turpin, B. J. and Lim, H.-J.: Species Contributions to PM2.5 Mass Concentrations: Revisiting Common Assumptions for Estimating Organic Mass, Aerosol Science and Technology, 35, 602-610, 10.1080/02786820119445, 2001.
Vignati, E., Karl, M., Krol, M., Wilson, J., Stier, P., and Cavalli, F.: Sources of uncertainties in modelling black carbon at the global scale, Atmos. Chem. Phys., 10, 2595-2611, 10.5194/acp-10-2595-2010, 2010.
Wang, J., Nie, W., Cheng, Y., Shen, Y., Chi, X., Wang, J., Huang, X., Xie, Y., Sun, P., Xu, Z., Qi, X., Su, H., and Ding, A.: Light absorption of brown carbon in eastern China based on 3-year multi-wavelength aerosol optical property observations and an improved absorption Ångström exponent segregation method, Atmos. Chem. Phys., 18, 9061-9074, 10.5194/acp-18-9061-2018, 2018.
Watson, J. G., Chow, J. C., and Chen, L. W. A.: Summary of Organic and Elemental Carbon/Black Carbon Analysis Methods and Intercomparisons, Aerosol and Air Quality Research, 5, 65-102, 10.4209/aaqr.2005.06.0006, 2005.
WHO: Health impact of ambient air pollution in Serbia: A call to action, WHO, 2019.
WHO: WHO global air quality guidelines. Particulate matter (PM2.5 and PM10), ozone, nitrogen dioxide, sulfur dioxide and carbon monoxide. Licence: CC BY□NC□SA 3.0 IGO., World Health Organization, Geneva, 2021.
Wong, J. P. S., Tsagkaraki, M., Tsiodra, I., Mihalopoulos, N., Violaki, K., Kanakidou, M., Sciare, J., Nenes, A., and Weber, R. J.: Atmospheric evolution of molecular-weight-separated brown carbon from biomass burning, Atmos. Chem. Phys., 19, 7319-7334, 10.5194/acp-19-7319-2019, 2019.
World Bank: Transport Inputs to the Western Balkans Green Growth Narrative Strategic Actions for a Greener and More Efficient Transport Sector Policy Note, 2024.
Yttri, K. E., Aas, W., Bjerke, A., Cape, J. N., Cavalli, F., Ceburnis, D., Dye, C., Emblico, L., Facchini, M. C., Forster, C., Hanssen, J. E., Hansson, H. C., Jennings, S. G., Maenhaut, W., Putaud, J. P., and Tørseth, K.: Elemental and organic carbon in PM₁₀: a one year measurement campaign within the European Monitoring and Evaluation Programme EMEP, Atmos. Chem. Phys., 7, 5711-5725, 10.5194/acp-7-5711-2007, 2007.
Yttri, K. E., Simpson, D., Nøjgaard, J. K., Kristensen, K., Genberg, J., Stenström, K., Swietlicki, E., Hillamo, R., Aurela, M., Bauer, H., Offenberg, J. H., Jaoui, M., Dye, C., Eckhardt, S., Burkhart, J. F., Stohl, A., and Glasius, M.: Source apportionment of the summer time carbonaceous aerosol at Nordic rural background sites, Atmos. Chem. Phys., 11, 13339-13357, 10.5194/acp-11-13339-2011, 2011.
Yttri, K. E., Canonaco, F., Eckhardt, S., Evangeliou, N., Fiebig, M., Gundersen, H., Hjellbrekke, A. G., Lund Myhre, C., Platt, S. M., Prévôt, A. S. H., Simpson, D., Solberg, S., Surratt, J., Tørseth, K., Uggerud, H., Vadset, M., Wan, X., and Aas, W.: Trends, composition, and sources of carbonaceous aerosol at the Birkenes Observatory, northern Europe, 2001–2018, Atmos. Chem. Phys., 21, 7149-7170, 10.5194/acp-21-7149-2021, 2021.
Yttri, K. E., Bäcklund, A., Conen, F., Eckhardt, S., Evangeliou, N., Fiebig, M., Kasper-Giebl, A., Gold, A., Gundersen, H., Myhre, C. L., Platt, S. M., Simpson, D., Surratt, J. D., Szidat, S., Rauber, M., Tørseth, K., Ytre-Eide, M. A., Zhang, Z., and

https://doi.org/10.5194/egusphere-2026-1708
Preprint. Discussion started: 10 August 2026

Aas, W.: Composition and sources of carbonaceous aerosol in the European Arctic at Zeppelin Observatory, Svalbard (2017 to 2020), Atmos. Chem. Phys., 24, 2731-2758, 10.5194/acp-24-2731-2024, 2024.

Zangrando, R., Chiari, M., Vedernikov, A., Andreoli, R., Perrone, M. G., Possanzini, M., and Belis, C. A.: Source apportionment of PM2.5 organic aerosol in Belgrade (Serbia) by positive matrix factorization of organic tracers, Environmental Science and Pollution Research, 23, 15236-15248, 10.1007/s11356-016-6685-6, 2016a.

Zangrando, R., Barbaro, E., Kirchgeorg, T., Vecchiato, M., Scalabrin, E., Radaelli, M., Đorđević, D., Barbante, C., and Gambaro, A.: Five primary sources of organic aerosols in the urban atmosphere of Belgrade (Serbia), Science of The Total Environment, 571, 1441-1453, https://doi.org/10.1016/j.scitotenv.2016.06.188, 2016b.

Zhang, Q., Worsnop, D. R., Canagaratna, M. R., and Jimenez, J. L.: Hydrocarbon-like and oxygenated organic aerosols in Pittsburgh: insights into sources and processes of organic aerosols, Atmos. Chem. Phys., 5, 3289-3311, 10.5194/acp-5-3289-2005, 2005.

Zotter, P., Herich, H., Gysel, M., El-Haddad, I., Zhang, Y., Močnik, G., Hüglin, C., Baltensperger, U., Szidat, S., and Prévôt, A. S. H.: Evaluation of the absorption Ångström exponents for traffic and wood burning in the Aethalometer-based source apportionment using radiocarbon measurements of ambient aerosol, Atmos. Chem. Phys., 17, 4229-4249, 10.5194/acp-17-4229-2017, 2017.

Zotter, P., Ciobanu, V. G., Zhang, Y. L., El-Haddad, I., Macchia, M., Daellenbach, K. R., Salazar, G. A., Huang, R. J., Wacker, L., Hueglin, C., Piazzalunga, A., Fermo, P., Schwikowski, M., Baltensperger, U., Szidat, S., and Prévôt, A. S. H.: Radiocarbon analysis of elemental and organic carbon in Switzerland during winter-smog episodes from 2008 to 2012 – Part 1: Source apportionment and spatial variability, Atmos. Chem. Phys., 14, 13551-13570, 10.5194/acp-14-13551-2014, 2014.